Electronic Supporting information (ESI)

Table of Contents

Characterization

The diffuse reflectance data were converted to absorbance data employing the Kubelka−Munk[1] function by using the equation (1)

$$F(R) = \frac{(1-R)^2}{2R} = \frac{\alpha}{S} \quad \ldots\ldots\ldots\ldots(1)$$

in which R is the reflectance, α is absorptivity, and S is the scattering factor.

The optical band gaps were calculated from Tauc plots.[2] The Tauc relation (2) is

$$\alpha h\nu = A(h\nu - Eg)n \quad \ldots\ldots\ldots\ldots(2)$$

where α is absorption coefficient, A is a constant called the band tailing parameter, and n is the power factor of the transition mode. The plot of $(\alpha h\nu)^{(1/n)}$ versus the photon energy (hv) gives a straight line in a certain region.[3] The extrapolation of this straight line intercepts the (hv)-axis to give the value of the optical band gap (E_g).

The working electrode was prepared by mixing 4 mg of the catalyst along with 1 mg of carbon black dispersed in 3:1 ratio of isopropanol and water mixture and 0.04 mL of Nafion. This suspension was ultrasonicated for 1-2 h to obtain a homogeneous mixture. This gave a loading of 0.255 mg/cm^2 of the catalyst. All the parameters were converted to reversible hydrogen electrode (RHE) scale using the Nernst equation[4] (equation 3). The overpotential (η) was calculated using the formula

$$E_{RHE} = E_{Hg/HgO} + E^0_{Hg/HgO} + 0.059*pH \quad \ldots\ldots\ldots.(3)$$

$$\eta = E_{RHE} - 1.23 \quad \ldots\ldots\ldots.. (4)$$

Both overpotential (η) (thermodynamic parameter) and exchange current density (j_0) (kinetic parameter) of the electrochemical reaction analysed by Butler-Volmer equation (equation 5). The Tafel analysis ($log|i| \ vs \ \eta_i$), when electrochemical reaction not in equilibrium (equation 6). This Tafel plot helps to understand the kinetics of the reaction.

$$i = i_0 \left(c_O e^{\frac{\alpha_c n_e F\eta}{RT}} - c_R e^{\frac{\alpha_a n_e F\eta}{RT}} \right) \quad \ldots\ldots\ldots\ldots.(5)$$

$$log|i| = log|i_0| + (\alpha nF/2.303RT)\eta_i \quad \ldots\ldots\ldots\ldots.(6)$$

In the above equation, η,R,T,α,n,F and j indicate overpotential, gas constant, temperature in K, charge-transfer coefficient, number of electrons transferred per molecule of product formed during reaction and current density respectively.[5]
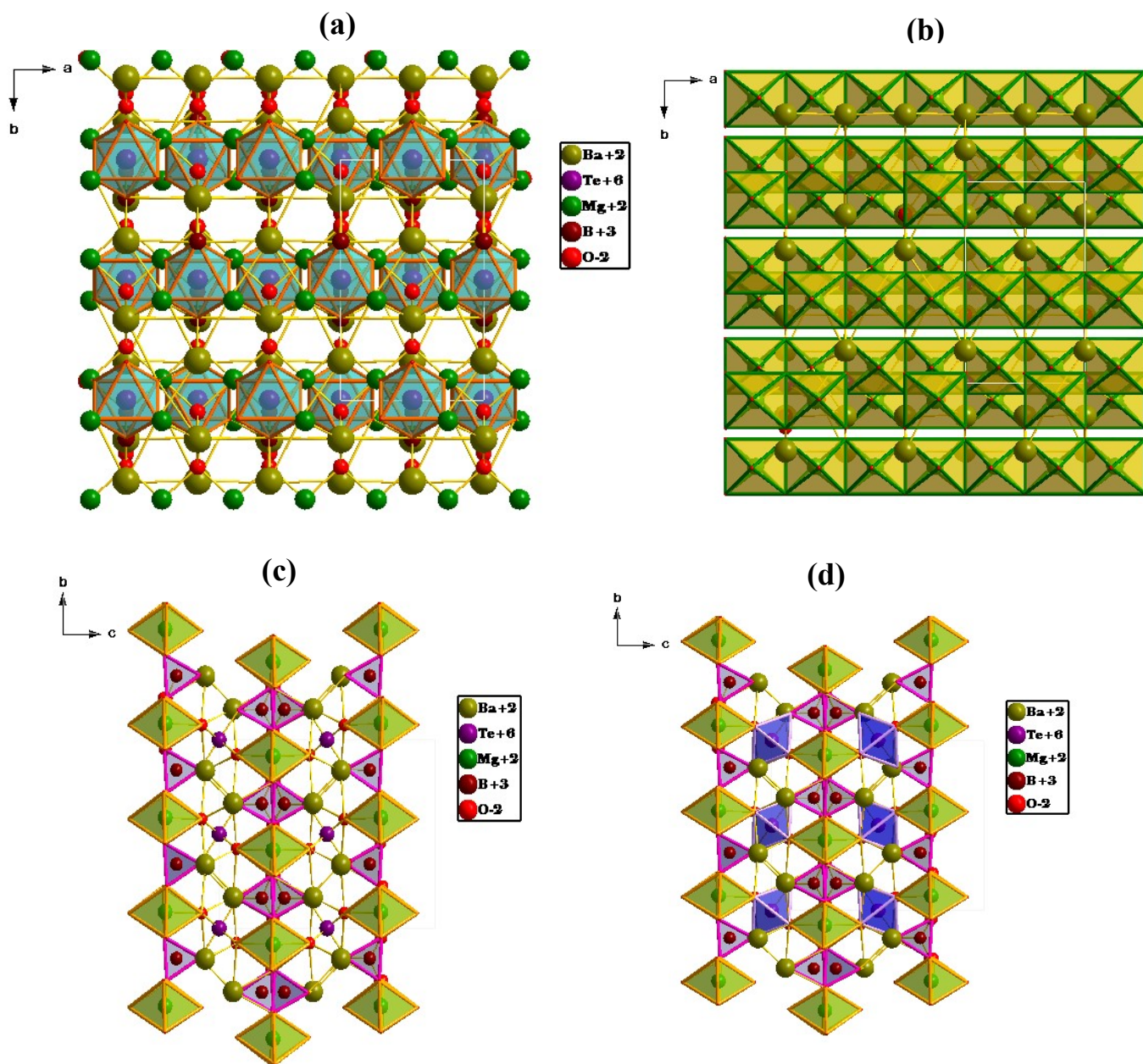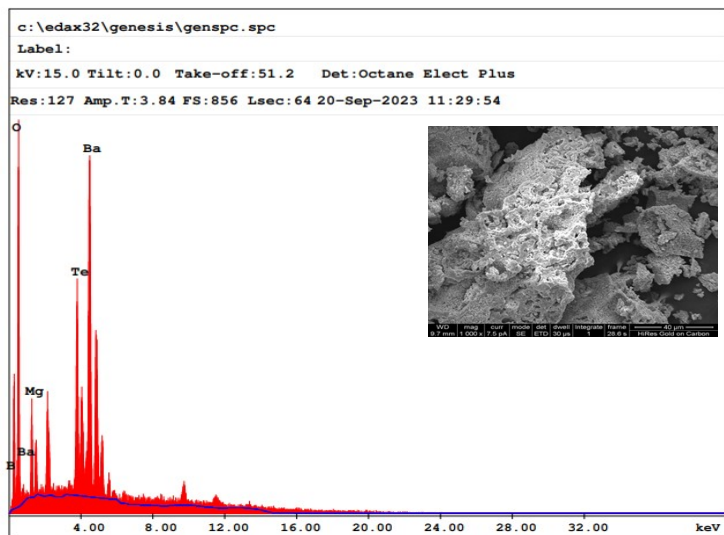
(a)

(b)

(c)

(d)

Figure S1. Crystal structure of $Ba_2Mg_2TeB_2O_{10}$ drawn from the Rietveld refinement data.

$Ba_2Mg_2TeB_2O_{10}$

Elements	Atomic weight (u)	Weight percentage (calculated)	Weight percentage (observed)	Atomic percentage (calculated)	Atomic percentage (observed)	Weight percentage /Atomic weight
Ba L	137.327	43.425	64.07	11.765	34.60	0.3162
Mg K	24.305	7.685	02.71	11.765	08.28	0.3162
Te L	127.60	20.174	24.44	05.882	14.21	0.1581
B K	10.811	3.418	01.00	11.761	06.85	0.3161
O K	15.999	25.295	07.78	58.825	36.06	1.581
Total	632.476	100		100		2.6876
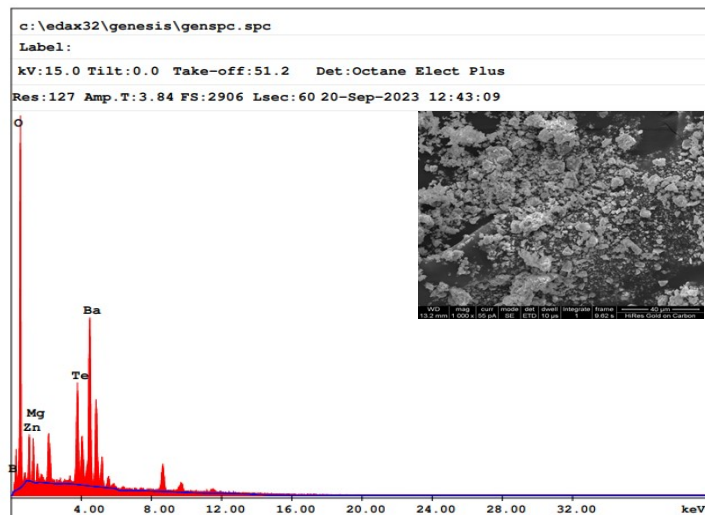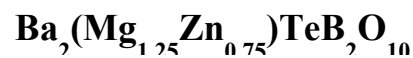
$Ba_2(Mg_{1.25}Zn_{0.75})TeB_2O_{10}$

Elements	Atomic weight (u)	Weight percentage (calculated)	Weight percentage (observed)	Atomic percentage (calculated)	Atomic percentage (observed)	Weight percentage /Atomic weight
Ba L	137.327	41.400	56.06	11.767	23.62	0.30147
Mg K	24.305	4.580	02.12	07.355	05.06	0.18843
Zn L	65.380	7.390	05.00	04.412	04.43	0.11303
Te L	127.60	19.230	21.73	05.882	09.86	0.15070
B K	10.811	3.250	01.43	11.734	07.64	0.30061
O K	15.999	24.120	13.66	58.848	49.40	1.50759
Total	673.551	100		100		2.56183
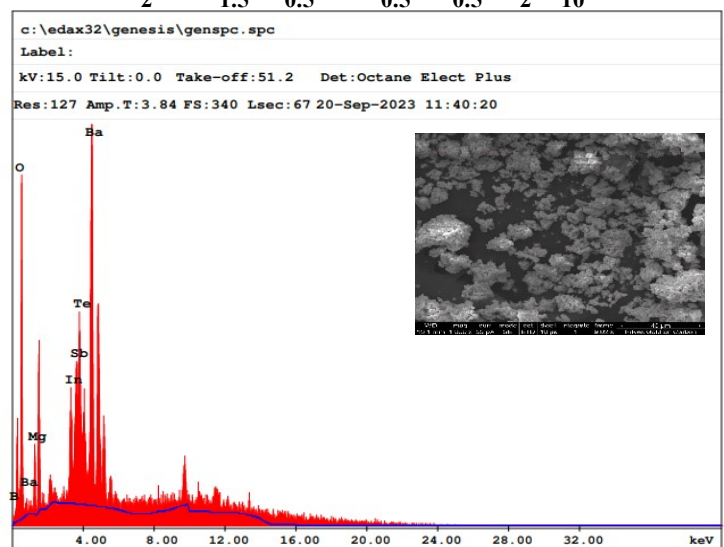
$Ba_2(Mg_{1.5}In_{0.5})(Te_{0.5}Sb_{0.5})B_2O_{10}$

Elements	Atomic weight (u)	Weight percentage (calculated)	Weight percentage (observed)	Atomic percentage (calculated)	Atomic percentage (observed)	Weight percentage /Atomic weight
Ba L	137.327	40.700	56.38	11.764	34.20	0.2963
Mg K	24.305	5.402	01.47	8.822	05.04	0.2222
In L	114.818	8.507	07.67	2.938	05.56	0.0740
Sb L	121.760	9.021	12.91	2.938	08.84	0.0740
Te L	127.60	9.454	14.87	2.938	09.71	0.0740
B K	10.811	3.204	00.69	11.764	05.30	0.2963

$Ba_2(MgCo)TeB_2O_{10}$

Elements	Atomic weight (u)	Weight percentage (calculated)	Weight percentage (observed)	Atomic percentage (calculated)	Atomic percentage (observed)	Weight percentage /Atomic weight
Ba L	137.327	41.171	52.72	11.767	25.00	0.2998
Mg K	24.305	3.643	01.69	5.879	04.52	0.1498
Co K	58.933	8.834	14.30	5.879	15.80	0.1498
Te L	127.60	19.127	20.99	5.879	10.71	0.1498
B K	10.811	3.241	01.06	11.763	06.37	0.2997

S6

Ba$_2$(Mg$_{1.5}$Ni$_{0.5}$)TeB$_2$O$_{10}$


```
c:\edax32\genesis\genspc.spc
Label:
kV:15.0 Tilt:0.0 Take-off:51.2   Det:Octane Elect Plus
Res:127 Amp.T:3.84 FS:1136 Lsec:61 20-Sep-2023 12:16:24
```

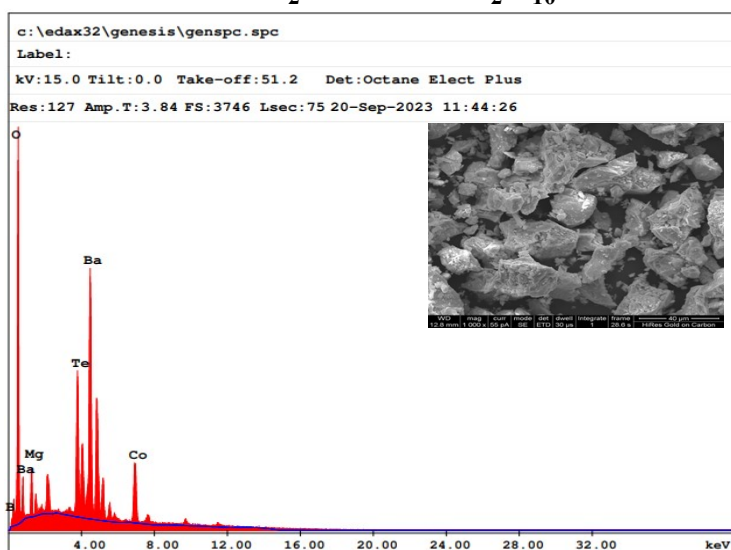| Elements	Atomic weight (u)	Weight percentage (calculated)	Weight percentage (observed)	Atomic percentage (calculated)	Atomic percentage (observed)	Weight percentage /Atomic weight
Ba L	137.327	42.275	50.41	11.766	19.03	0.3078
Mg K	24.305	5.611	03.36	8.822	07.15	0.2308
Ni L	58.693	4.517	11.00	2.924	09.71	0.0765
Te L	127.60	19.640	18.70	5.883	07.60	0.1539
B K	10.811	3.328	01.89	11.766	09.06	0.3078
O K	15.999	24.626	14.64	58.837	47.44	1.5392
Total	649.670	100		100		2.616

Ba$_2$(Mg$_{1.5}$Cu$_{0.5}$)TeB$_2$O$_{10}$


```
c:\edax32\genesis\genspc.spc
Label:
kV:15.0 Tilt:0.0 Take-off:51.2   Det:Octane Elect Plus
Res:127 Amp.T:3.84 FS:2502 Lsec:61 20-Sep-2023 12:11:33
```
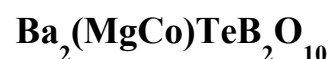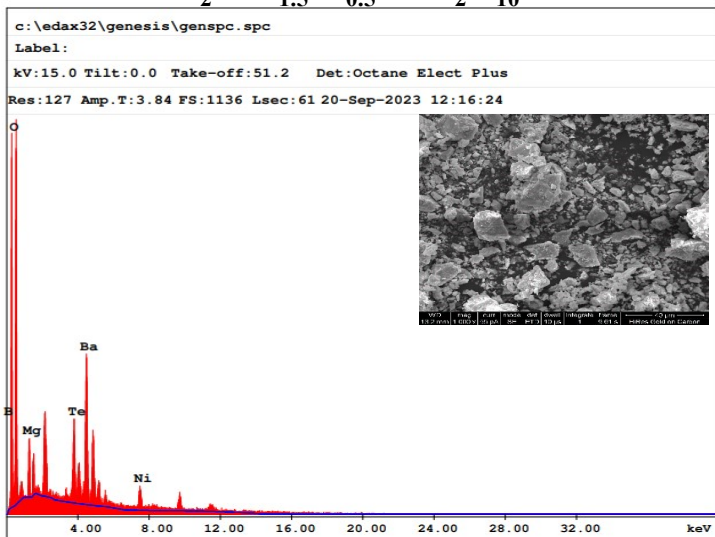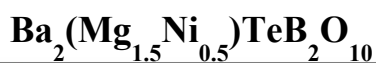
Elements	Atomic weight (u)	Weight percentage (calculated)	Weight percentage (observed)	Atomic percentage (calculated)	Atomic percentage (observed)	Weight percentage /Atomic weight
Ba L	137.327	42.118	53.13	11.762	21.65	0.3066
Mg K	24.305	5.590	03.61	8.819	08.31	0.2299
Cu K	63.546	4.872	07.61	2.938	06.70	0.0766
Te L	127.60	19.567	21.00	5.881	09.21	0.1533
B K	10.811	3.315	01.73	11.762	08.96	0.3066
O K	15.999	24.537	12.91	58.835	45.16	1.5336
Total	652.096	100		100		2.6066

Ba$_2$(Mg$_{1.5}$Fe$_{0.5}$)TeB$_2$O$_{10}$


```
c:\edax32\genesis\genspc.spc
Label:
kV:15.0 Tilt:0.0 Take-off:51.2   Det:Octane Elect Plus
Res:127 Amp.T:3.84 FS:1918 Lsec:72 20-Sep-2023 12:07:35
```
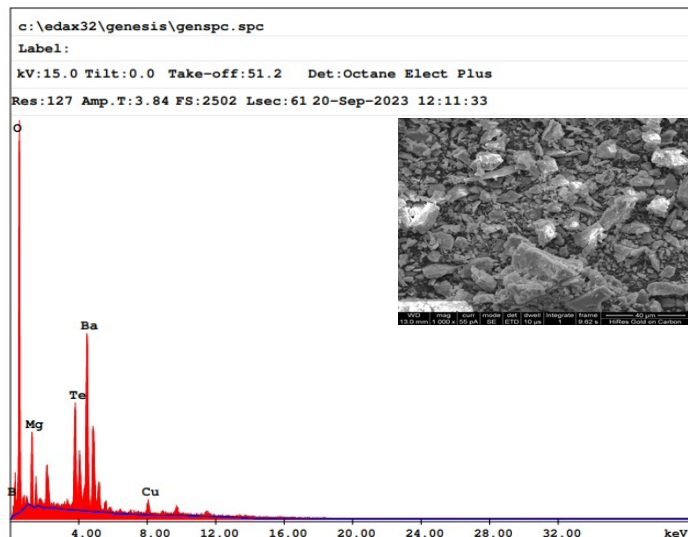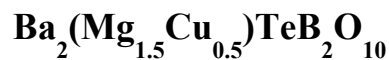
Elements	Atomic weight (u)	Weight percentage (calculated)	Weight percentage (observed)	Atomic percentage (calculated)	Atomic percentage (observed)	Weight percentage /Atomic weight
Ba L	137.327	42.368	62.70	11.764	35.98	0.30851
Mg K	24.305	05.624	01.83	08.823	05.92	0.23139
Fe K	55.845	04.307	04.02	02.940	05.67	0.07712
Te L	127.60	19.683	24.09	05.882	14.88	0.15425
B K	10.811	03.335	0.54	11.763	03.90	0.30848
O K	15.999	24.680	06.83	58.824	33.65	1.54259

(Ba$_{0.5}$Pb$_{1.5}$)Mg$_2$TeB$_2$O$_{10}$


```
c:\edax32\genesis\genspc.spc
Label:
kV:15.0 Tilt:0.0 Take-off:51.2   Det:Octane Elect Plus
Res:127 Amp.T:3.84 FS:3085 Lsec:64 20-Sep-2023 11:34:29
```
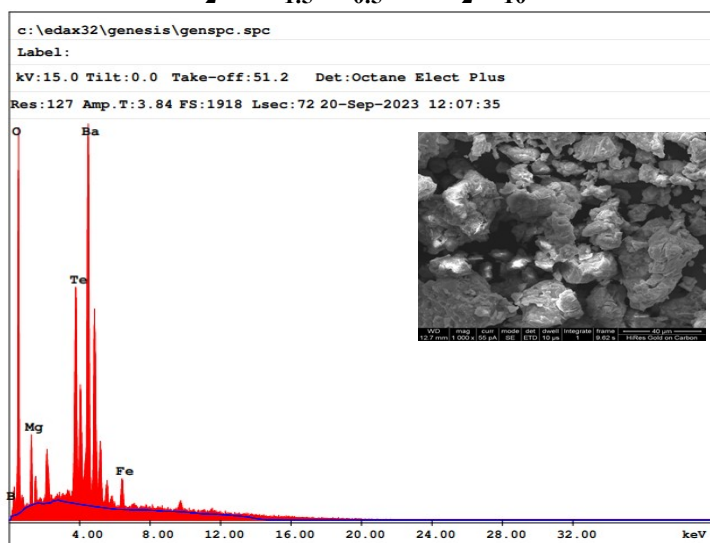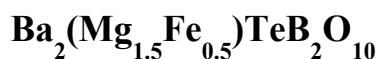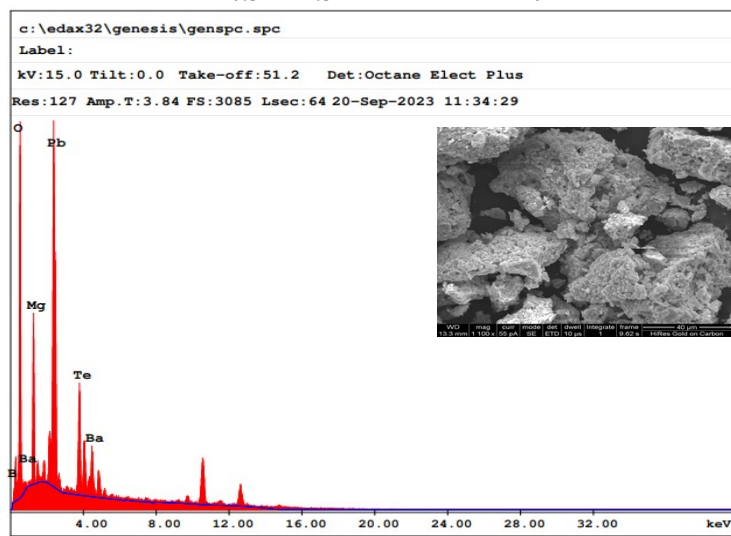
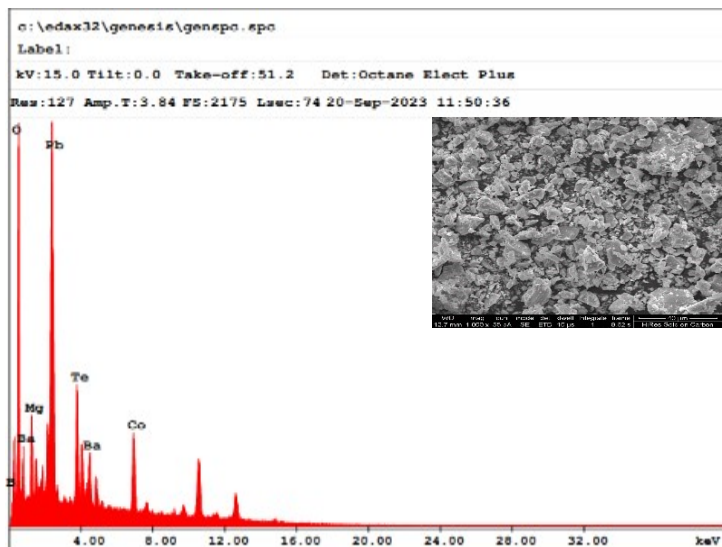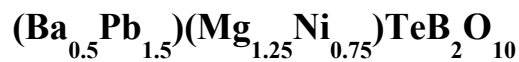| Elements	Atomic weight (u)	Weight percentage (calculated)	Weight percentage (observed)	Atomic percentage (calculated)	Atomic percentage (observed)	Weight percentage /Atomic weight
Ba L	137.327	9.313	12.92	02.940	05.10	0.0678
Pb M	207.2	42.154	42.36	08.820	11.09	0.2034
Mg K	24.305	6.593	05.81	11.761	12.95	0.2712
Te L	127.60	17.306	21.27	05.88	09.04	0.1356
B K	10.811	2.932	01.24	11.761	06.22	0.2712
O K	15.999	21.699	16.40	58.00	55.60	1.3562

$(Ba_{0.5}Pb_{1.5})(MgCo)TeB_2O_{10}$

Elements	Atomic weight (u)	Weight percentage (calculated)	Weight percentage (observed)	Atomic percentage (calculated)	Atomic percentage (observed)	Weight percentage /Atomic weight
Ba L	137.327	8.895	12.45	2.938	05.26	0.0647
Pb M	207.2	40.263	35.73	8.815	10.01	0.1941
Mg K	24.305	3.148	02.15	5.881	05.12	0.1295
Co K	58.933	7.634	16.82	5.881	16.58	0.1295
Te L	127.60	16.530	18.58	5.881	08.45	0.1295
B K	10.811	2.801	01.58	11.763	08.49	0.2590
O K	15.999	20.726	12.70	58.836	46.09	1.2954
Total	771.913	100		100		2.2017

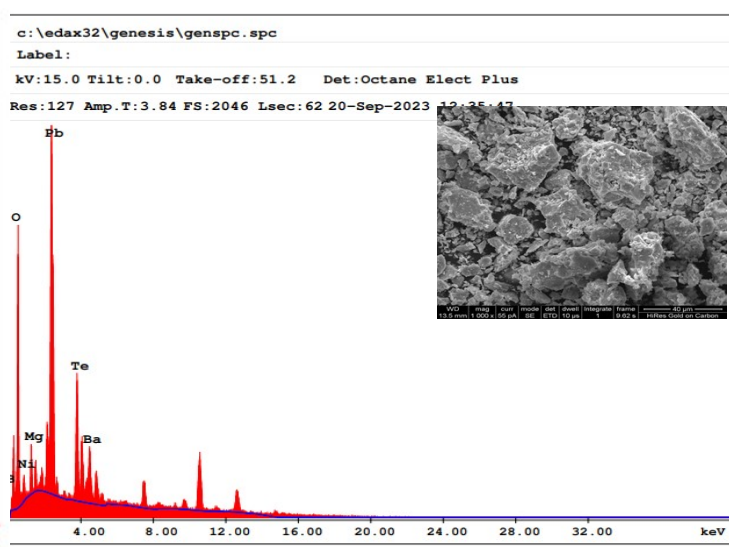## $(Ba_{0.5}Pb_{1.5})(Mg_{1.25}Ni_{0.75})TeB_2O_{10}$

Elements	Atomic weight (u)	Weight percentage (calculated)	Weight percentage (observed)	Atomic percentage (calculated)	Atomic percentage (observed)	Weight percentage /Atomic weight
Ba L	137.327	8.998	15.03	2.940	07.33	0.0655
Pb M	207.2	40.729	42.93	8.822	13.87	0.1965
Mg K	24.305	3.981	01.69	7.349	04.66	0.1637
Ni K	58.693	5.768	03.54	4.408	04.03	0.0982
Te L	127.60	16.721	23.61	5.881	12.39	0.1310
B K	10.811	2.833	01.23	11.763	07.60	0.2620
O K	15.999	20.966	11.98	58.833	50.12	1.3104
Total	763.076	100		100		2.2273

Figure S2. SEM-EDX spectra of $Ba_2(Mg_{2-x}M_x)TeB_2O_{10}$ (M=Zn, Co, Ni, Fe, Cu) and $(Ba_{0.5}Pb_{1.5})(Mg_{2-x}M_x)TeB_2O_{10}$ (M= Co, Ni, Cu).

Table S1. Nuclear site group analysis for each atom in $A_2Mg_2TeB_2O_{10}$ (A=Ba/Pb)

SI. No	Atom	Wyckoff position	Transformation in irreducible representations							
			A_g	B_{1g}	B_{2g}	B_{3g}	A_u	B_{1u}	B_{2u}	B_{3u}
1	Ba1/Pb1	8f	2	1	1	2	1	2	2	1
2	Mg1	8e	1	2	1	2	1	2	1	2
3	Te1	4a	0	0	0	0	1	2	2	1
4	B1	8f	2	1	1	2	1	2	2	1
5	O1	8f	2	1	1	2	1	2	2	1
6	O2	16g	3	3	3	3	3	3	3	3
7	O3	8f	2	1	1	2	1	2	2	1
8	O4	8f	2	1	1	2	1	2	2	1

From the reported X-ray diffraction data, the structure of $A_2Mg_2TeB_2O_{10}$ (A=Ba/Pb) consists of Ba1/Pb1, B1, O1, O3 and O4 atoms occupying 8f Wyckoff position, 8e Wyckoff position is occupied by Mg1, 4a Wyckoff position is occupied by Te1 and 16g Wyckoff position is occupied by O2 atom. The nuclear site group analysis described by Rousseau *et al* for the space group[6] *Cmca*, it gives the point group symmetry for all Wyckoff positions and the transformation in the corresponding irreducible representations. The transformations obtained in irreducible representations with the Wyckoff position of atoms are tabulated in Table <u>S1</u>. The total transformations are as follows:

Γ (102) = 14 A_g + 10 A_u + 10 B_{1g} + 17 B_{1u} + 9 B_{2g} + 16 B_{2u} + 15 B_{3g} + 11 B_{3u}

Γ_{Raman} (48) = 14A_g + 10B_{1g} + 9B_{2g} + 15B_{3g};

Γ_{IR} (41) = 16B_{1u} + 15B_{2u} + 10B_{3u};

Acoustic = B_{1u}+ B_{2u} + B_{3u};

Silent = 10A_u.

Some of the expected Raman bands were not observed may be due to very less intensity and overlapping with modes due to accidental degeneracy.[7] The molecular polarizability could be obtained by the Shannon's additive rule.[8]

$\alpha(Ba_{2-x}Pb_x)Mg_2TeB_2O_{10} = (2-x)\alpha(Ba^{2+})+(x)\alpha(Pb^{2+})+(2)\alpha(Mg^{2+})+\alpha(Te^{6+})+2\alpha(B^{3+})+10\ \alpha(O^{2-})$

The ion dielectric polarizabilities value for α (Ba^{2+}) = 6.40 $Å^3$; α (Pb^{2+}) = 6.58 $Å^3$; α (Te^{6+}) = 5.23 $Å^3$; α (Mg^{2+}) = 1.32 $Å^3$; α (B^{3+}) = 0.05 $Å^3$; α (O^{2-}) = 2.01 $Å^3$.

Table S2. The observed Raman vibrational bands correspond to BaO_{11}, MgO_6, MO_6 (M – Zn, Co, Ni, Cu, Fe, In), TeO_6, BO_3 polyhedra.

Name of the compound		Ba-O bond Vibration (cm^{-1})	Pb-O bond Vibration (cm^{-1})
$Ba_2Mg_2TeB_2O_{10}$		764	--------
$Ba_2(Mg_{1.25}Zn_{0.75})TeB_2O_{10}$		769	--------
$Ba_2(MgCo)TeB_2O_{10}$	$Ba^{2+}O_{11}$	770	--------
$Ba_2(Mg_{1.5}Ni_{0.5})TeB_2O_{10}$		768	--------
$Ba_2(Mg_{1.5}Cu_{0.5})TeB_2O_{10}$		767	--------
$Ba_2(Mg_{1.5}Fe_{0.5})TeB_2O_{10}$		724	--------
$Ba_2(Mg_{1.5}In_{0.5})(Te_{0.5}Sb_{0.5})B_2O_{10}$		763	--------
$(Ba_{0.5}Pb_{1.5})Mg_2TeB_2O_{10}$	$Pb^{2+}O_5$	144	293
$(Ba_{0.5}Pb_{1.5})(MgCo)TeB_2O_{10}$	&	140	286
$(Ba_{0.5}Pb_{1.5})(Mg_{1.25}Ni_{0.75})TeB_2O_{10}$	$Ba^{2+}O_5$	145	291
$(Ba_{0.5}Pb_{1.5})(Mg_{1.75}Cu_{0.25})TeB_2O_{10}$		144	290

Name of the compound		Symmetric stretching (cm^{-1})	Asymmetric stretching (cm^{-1})	Bending mode (cm^{-1})
$Ba_2Mg_2TeB_2O_{10}$		461	679	222
$Ba_2(Mg_{1.25}Zn_{0.75})TeB_2O_{10}$		460	678	217
$Ba_2(MgCo)TeB_2O_{10}$		458	673	212
$Ba_2(Mg_{1.5}Ni_{0.5})TeB_2O_{10}$		461	678	211
$Ba_2(Mg_{1.5}Cu_{0.5})TeB_2O_{10}$		460	679	219
$Ba_2(Mg_{1.5}Fe_{0.5})TeB_2O_{10}$	$Mg^{2+}O_6$	458	678	216
$Ba_2(Mg_{1.5}In_{0.5})(Te_{0.5}Sb_{0.5})B_2O_{10}$		456	677	217
$(Ba_{0.5}Pb_{1.5})Mg_2TeB_2O_{10}$		451	683	220
$(Ba_{0.5}Pb_{1.5})(MgCo)TeB_2O_{10}$		440	670	204
$(Ba_{0.5}Pb_{1.5})(Mg_{1.25}Ni_{0.75})TeB_2O_{10}$		448	680	219
$(Ba_{0.5}Pb_{1.5})(Mg_{1.75}Cu_{0.25})TeB_2O_{10}$		449	682	217

Name of the compound		Symmetric stretching (cm^{-1})	Asymmetric stretching (cm^{-1})	Bending mode (cm^{-1})
$Ba_2(Mg_{1.25}Zn_{0.75})TeB_2O_{10}$	$Zn^{2+}O_6$	398	239	344
$Ba_2(MgCo)TeB_2O_{10}$	$Co^{2+}O_6$	402	241	345
$(Ba_{0.5}Pb_{1.5})(MgCo)TeB_2O_{10}$	$Co^{2+}O_6$	411	243	357
$Ba_2(Mg_{1.5}Ni_{0.5})TeB_2O_{10}$	$Ni^{2+}O_6$	400	241	348
$(Ba_{0.5}Pb_{1.5})(Mg_{1.25}Ni_{0.75})TeB_2O_{10}$	$Ni^{2+}O_6$	408	243	338

Ba$_2$(Mg$_{1.5}$Cu$_{0.5}$)TeB$_2$O$_{10}$	Cu^{2+}O$_6$	398	220	307
(Ba$_{0.5}$Pb$_{1.5}$)(Mg$_{1.75}$Cu$_{0.25}$)TeB$_2$O$_{10}$	Cu^{2+}O$_6$	414	244	335
Ba$_2$(Mg$_{1.5}$Fe$_{0.5}$)TeB$_2$O$_{10}$	Fe^{2+}O$_6$	524	345	303
Ba$_2$(Mg$_{1.5}$In$_{0.5}$)(Te$_{0.5}$Sb$_{0.5}$)B$_2$O$_{10}$	In^{3+}O$_6$	568	344	301
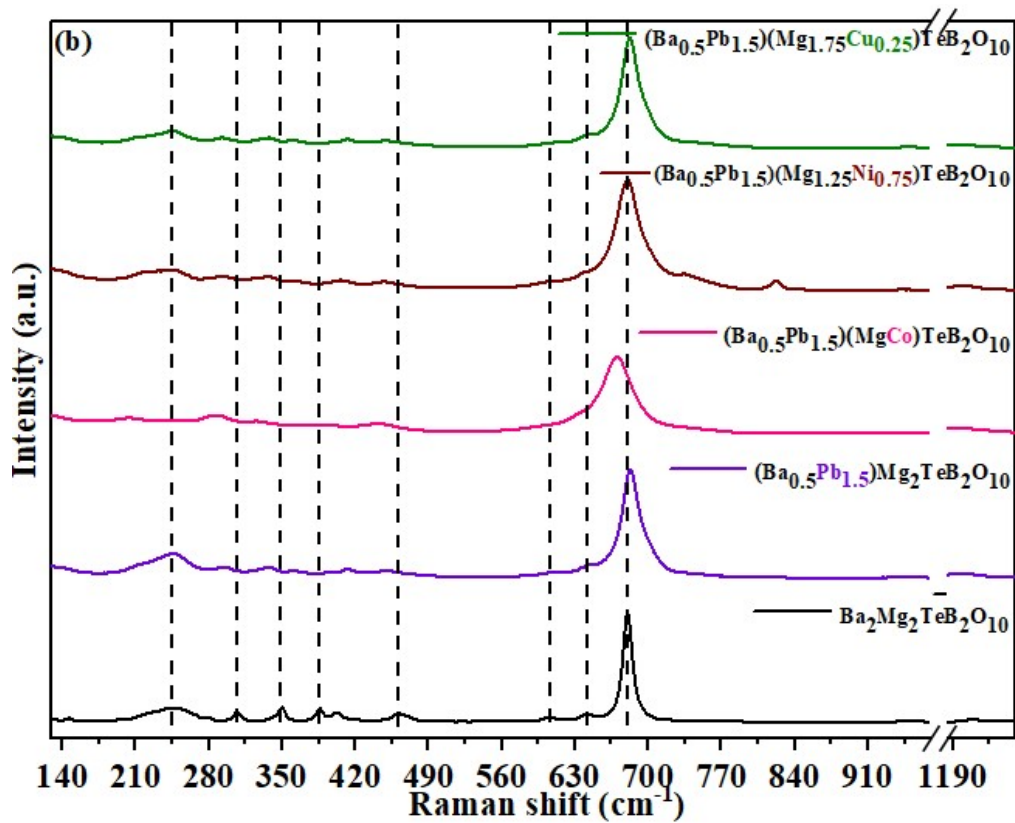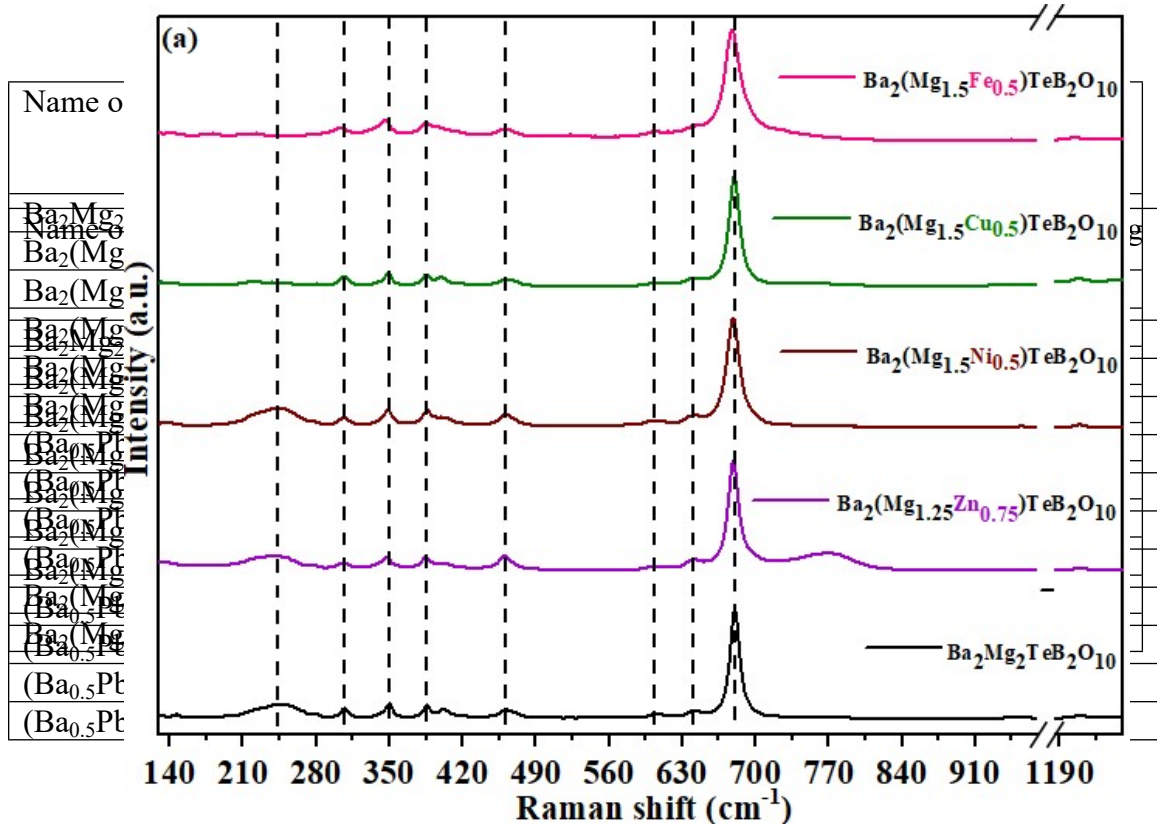
Figure S3. Raman spectra of (a) $Ba_2(Mg_{2-x}M_x)TeB_2O_{10}$ (M=Zn, Ni, Cu, Fe) and (b) $(Ba_{0.5}Pb_{1.5})(Mg_{2-x}M_x)TeB_2O_{10}$ (M= Co, Ni, Cu).
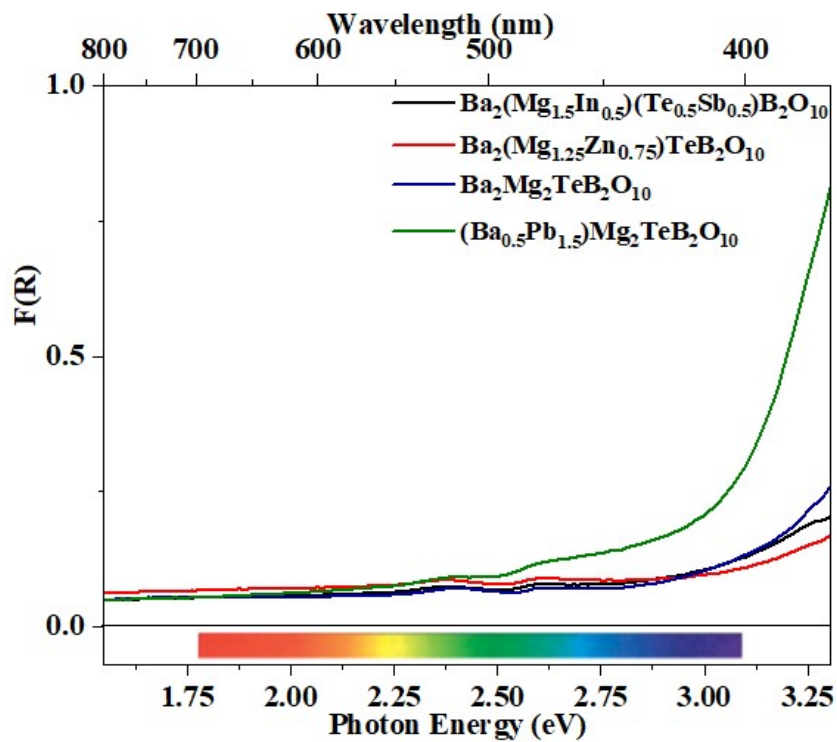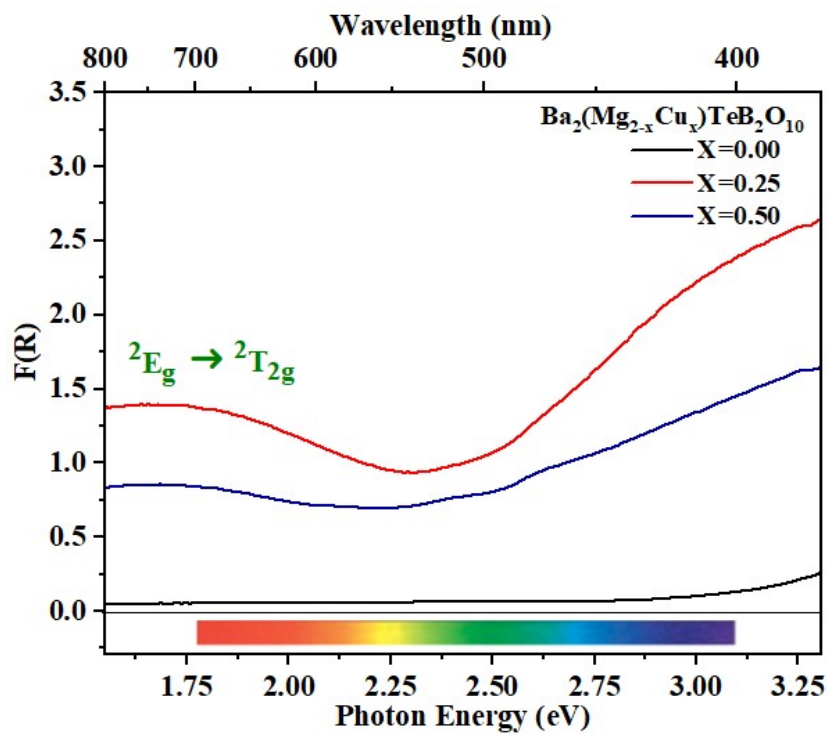
Figure S4. Optical absorption spectra for the prepared white-colored telluroborates.

Name of the compound	Band gap (eV) from Tauc plot
$Ba_2(Mg_{1.5}Cu_{0.5})TeB_2O_{10}$	1.91 eV

Figure S5. Optical absorption spectra for the $Ba_2(Mg_{2-x}Cu_x)TeB_2O_{10}$ ($0 < x \leq 0.5$).
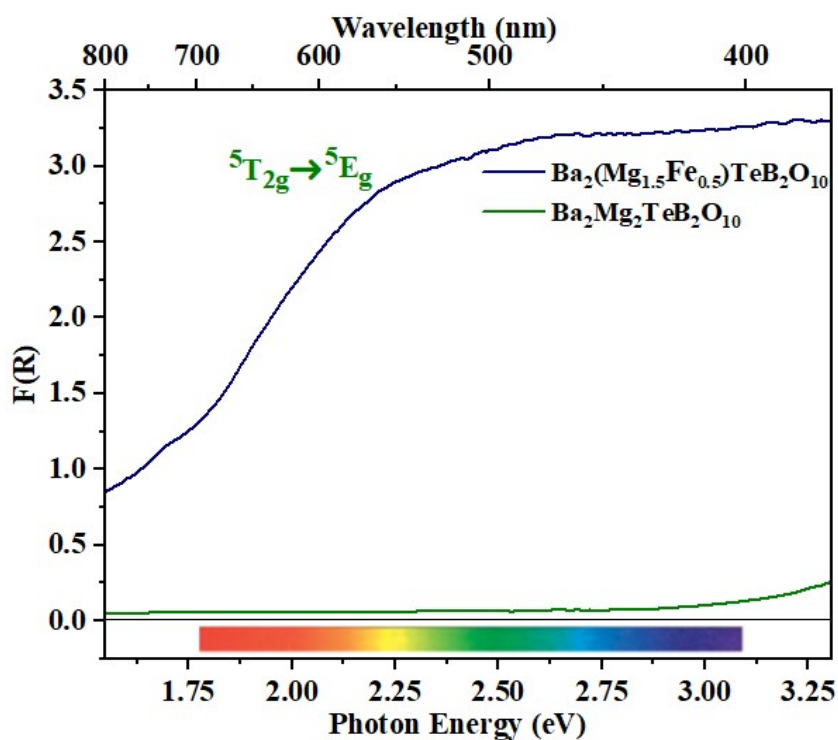
Figure S6. Optical absorption spectra for the $Ba_2(Mg_{2-x}Fe_x)TeB_2O_{10}$ $(0 < x \leq 0.5)$.
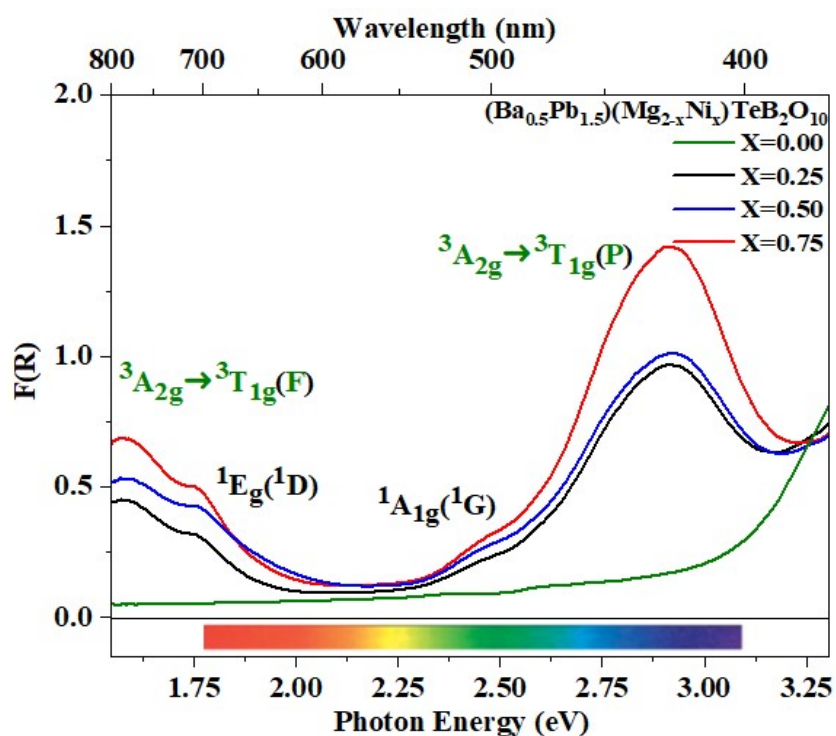
Figure S7. Optical absorption spectra for the $(Ba_{0.5}Pb_{1.5})(Mg_{2-x}Ni_x)TeB_2O_{10}$ $(0 < x \leq 0.75)$.
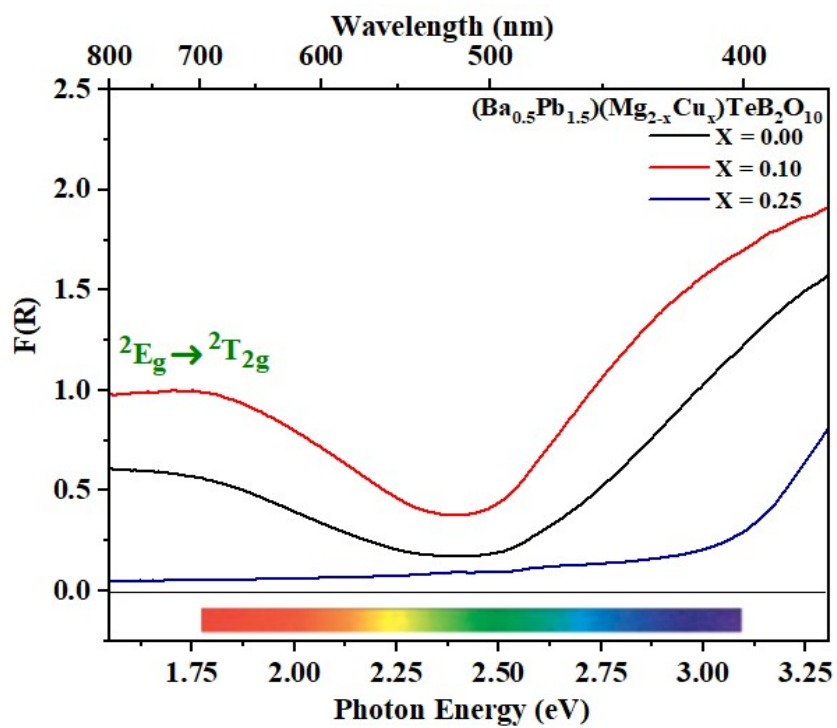
Figure S8. Optical absorption spectra for the $(Ba_{0.5}Pb_{1.5})(Mg_{2-x}Cu_x)TeB_2O_{10}$ $(0 < x \leq 0.25)$.

Table S3. Colors of $Ba_2(Mg_{2-x}M^{II}_x)TeB_2O_{10}$ (M^{II} = Fe, Co, Ni, and Cu) and $(Ba_{0.5}Pb_{1.5})(Mg_{2-}$

SI. No	Compounds	Ligand-field transitions (nm/eV)	Assignment*		Color
1	$Ba_2(Mg_{1.5}Fe_{0.5})TeB_2O_{10}$	551/2.25	$Fe^{2+}(3d^6)$	$^5T_{2g} \longrightarrow {}^5E_g$	
2	$Ba_2(MgCo)TeB_2O_{10}$	546/2.27	$Co^{2+}(3d^7)$	$^4T_{1g} \longrightarrow {}^4T_{1g}\,(^4P)$	
		742/1.67		$^4T_{1g} \longrightarrow {}^4A_{2g}\,(^4F)$	
3	$Ba_2(Mg_{1.5}Ni_{0.5})TeB_2O_{10}$	439/2.82	$Ni^{2+}(3d^8)$	$^3A_{2g}(^3F) \longrightarrow {}^3T_{1g}(^3P)$	
		815/1.52		$^3A_{2g}(^3F) \longrightarrow {}^3T_{1g}(^3F)$	
4	$Ba_2(Mg_{1.5}Cu_{0.5})TeB_2O_{10}$	708/1.75	$Cu^{2+}(3d^9)$	$^2E_g \longrightarrow {}^2T_{2g}$	
5	$(Ba_{0.5}Pb_{1.5})(MgCo)TeB_2O_{10}$	541/2.29	$Co^{2+}(3d^7)$	$^4T_{1g} \longrightarrow {}^4T_{1g}\,(^4P)$	
		689/1.80		$^4T_{1g} \longrightarrow {}^4A_{2g}\,(^4F)$	
6	$(Ba_{0.5}Pb_{1.5})(Mg_{1.25}Ni_{0.75})TeB_2O_{10}$	426/2.91	$Ni^{2+}(3d^8)$	$^3A_{2g}(^3F) \longrightarrow {}^3T_{1g}(^3P)$	
		789/1.57		$^3A_{2g}(^3F) \longrightarrow {}^3T_{1g}(^3F)$	
7	$(Ba_{0.5}Pb_{1.5})(Mg_{1.75}Cu_{0.25})TeB_2O_{10}$	700/1.77	$Cu^{2+}(3d^9)$	$^2E_g \longrightarrow {}^2T_{2g}$	

$_xM^{II}_x)TeB_2O_{10}$ (M^{II} = Co, Ni, and Cu) under Daylight.

*Ligand-field transitions, the assignments have been made for octahedral $M^{II}O_6$ chromophores given in refs [9–13]
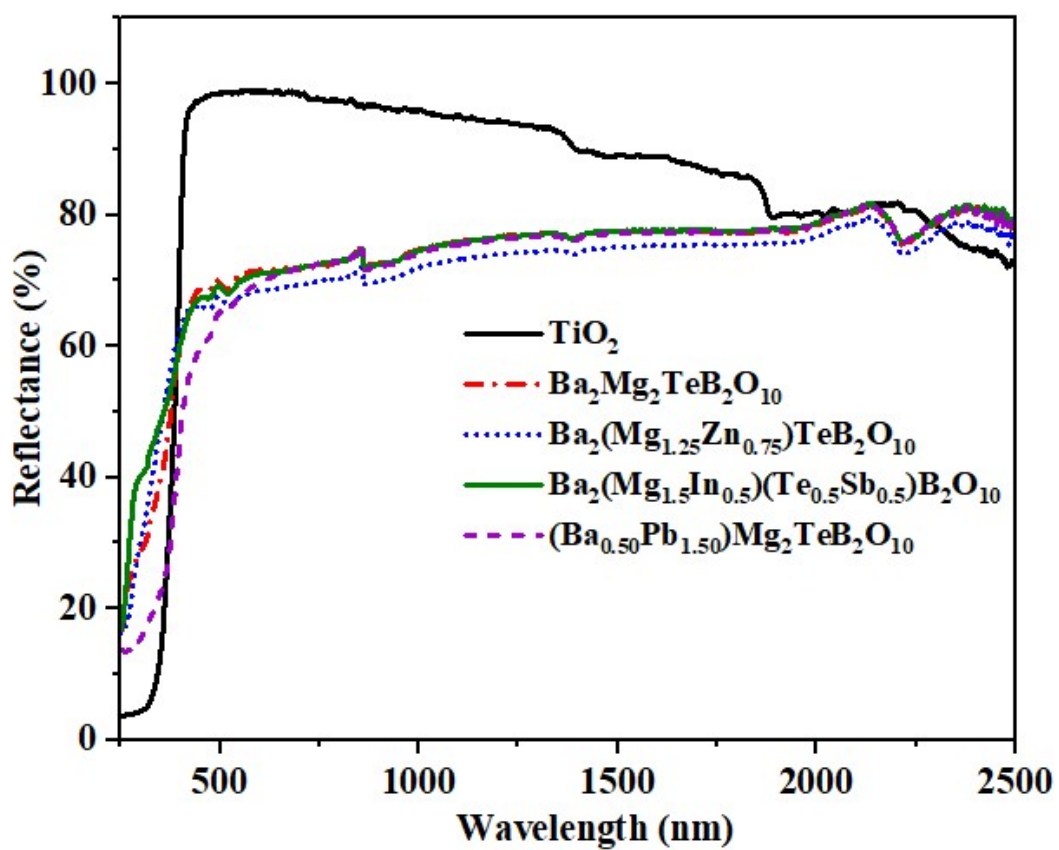
Figure S9. NIR reflectivity of the prepared white-colored telluroborates.
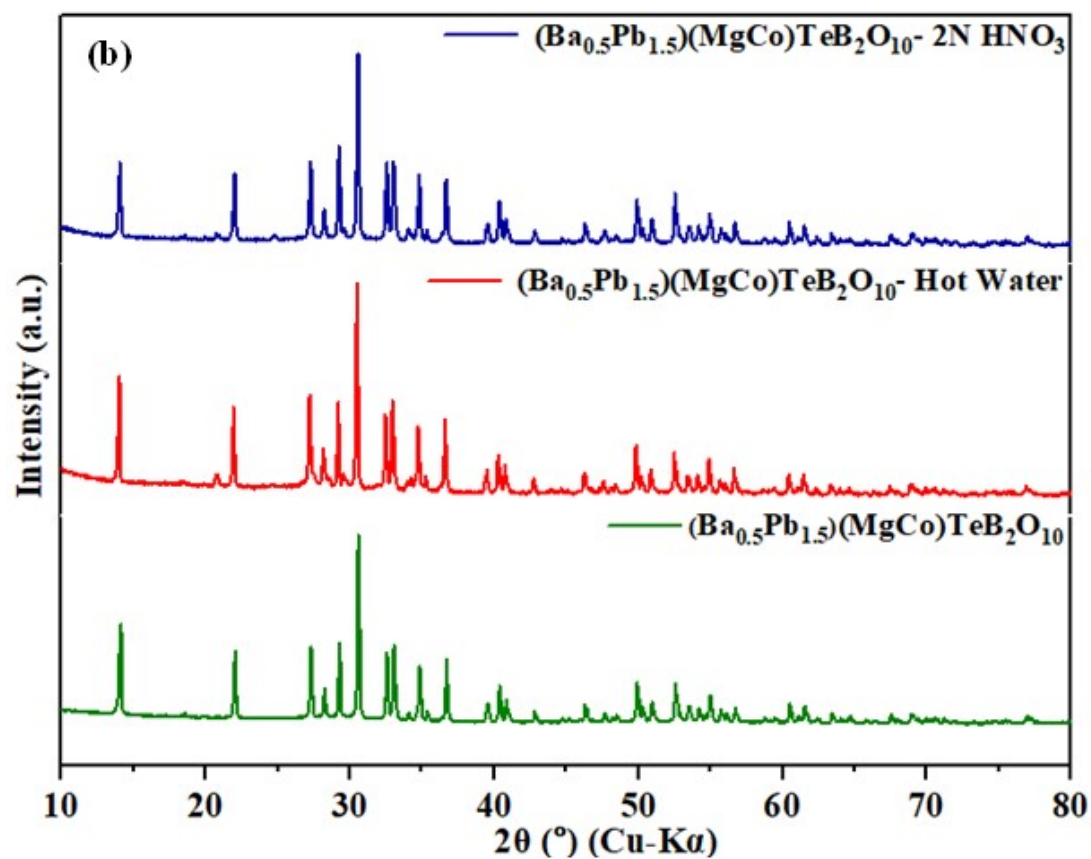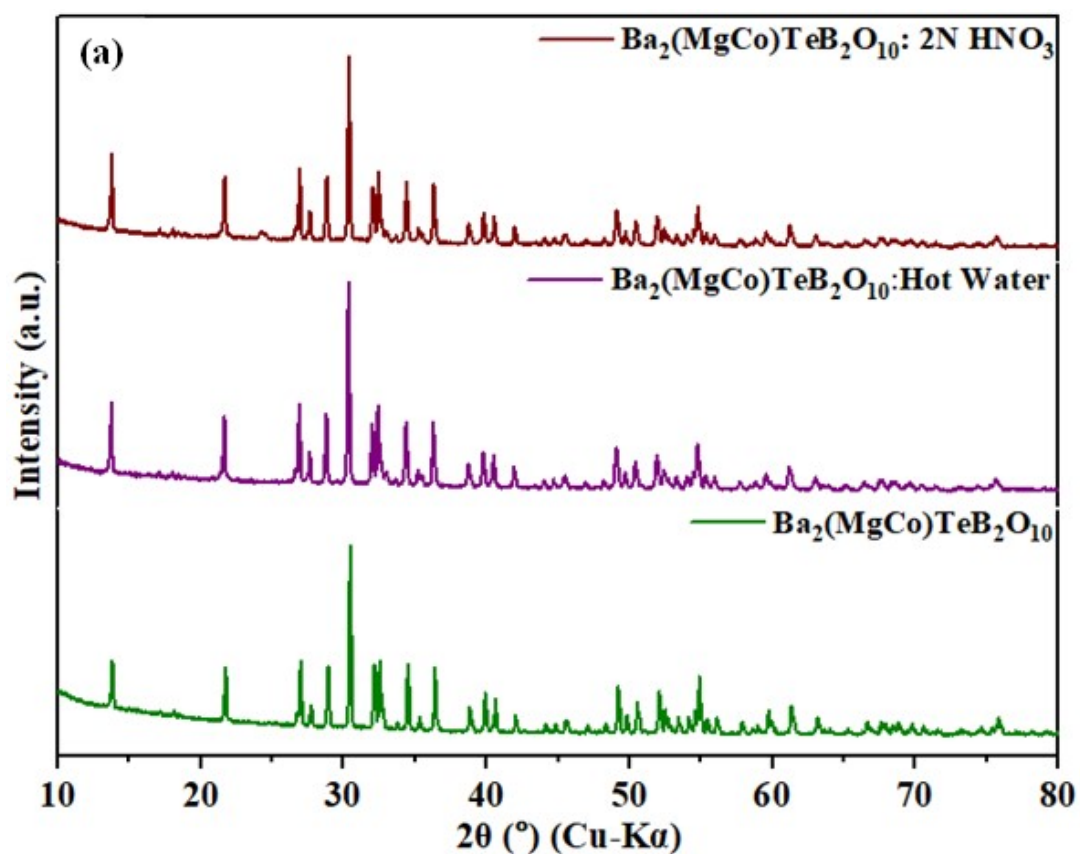
(Ba$_{0.5}$Pb$_{1.5}$)(MgCo)TeB$_2$O$_{10}$ after acid (2N HNO$_3$ solution) and hot water (24 h) treatment.
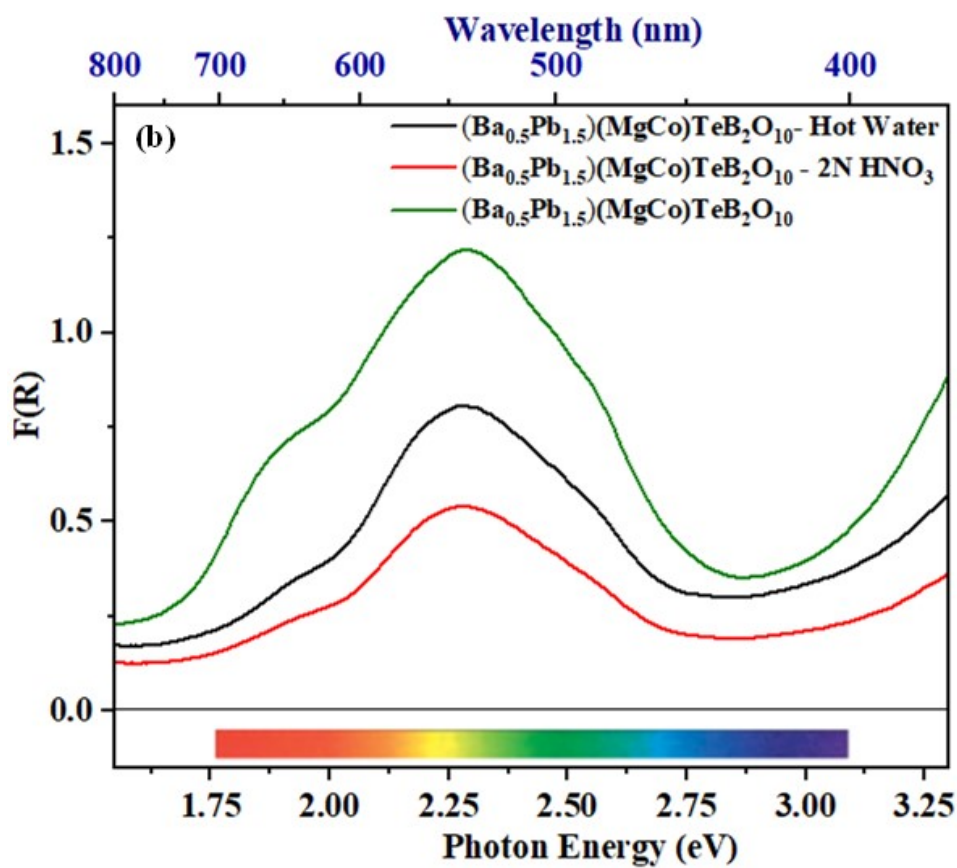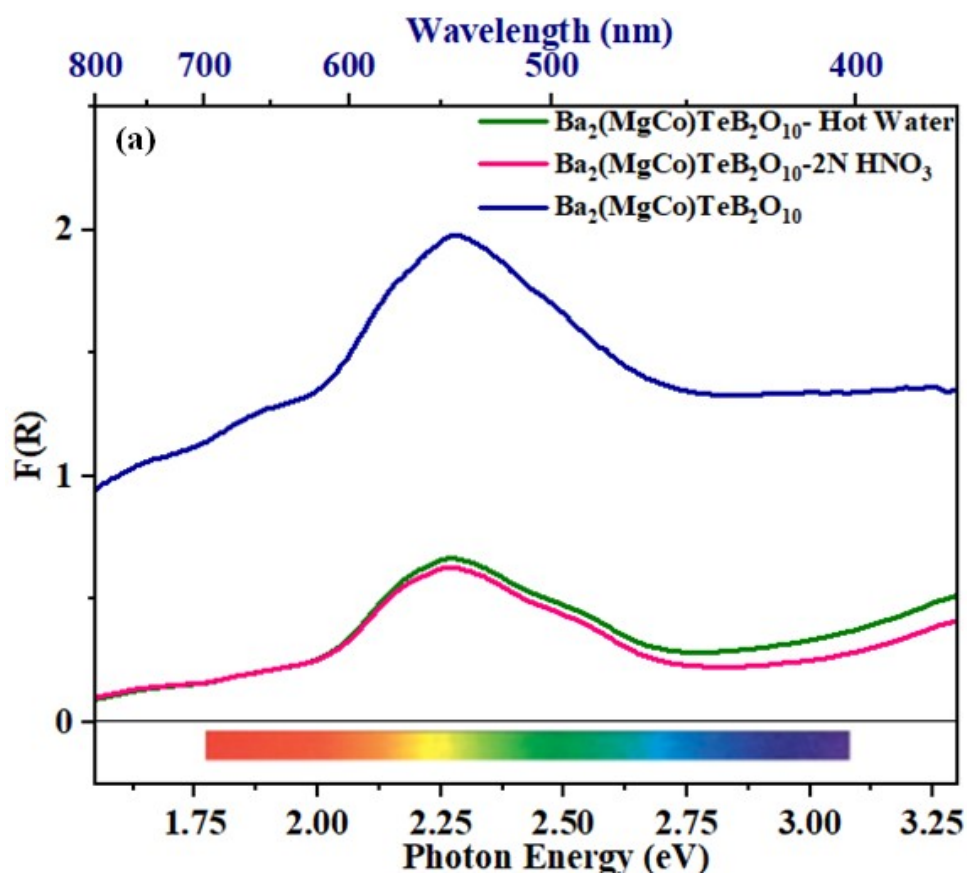
Figure S11. UV-Vis Spectra for acid and hot water stability of $Ba_2(MgCo)TeB_2O_{10}$ and $(Ba_{0.5}Pb_{1.5})(MgCo)TeB_2O_{10}$ after acid and hot water treatment.

$Ba_2(MgCo)TeB_2O_{10}$

$(Ba_{0.5}Pb_{1.5})(MgCo)TeB_2O_{10}$
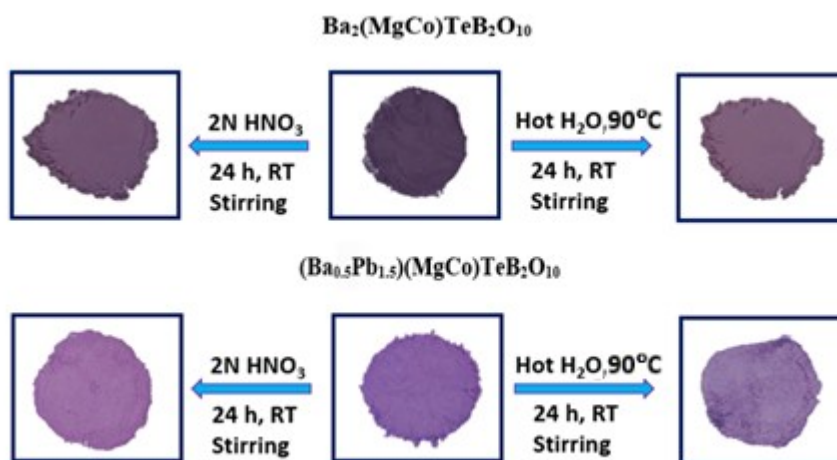
Figure S12. Color of the $(Ba_{2-x}Pb_x)(MgCo)TeB_2O_{10}$ before and after acid treatment, hot water stability.
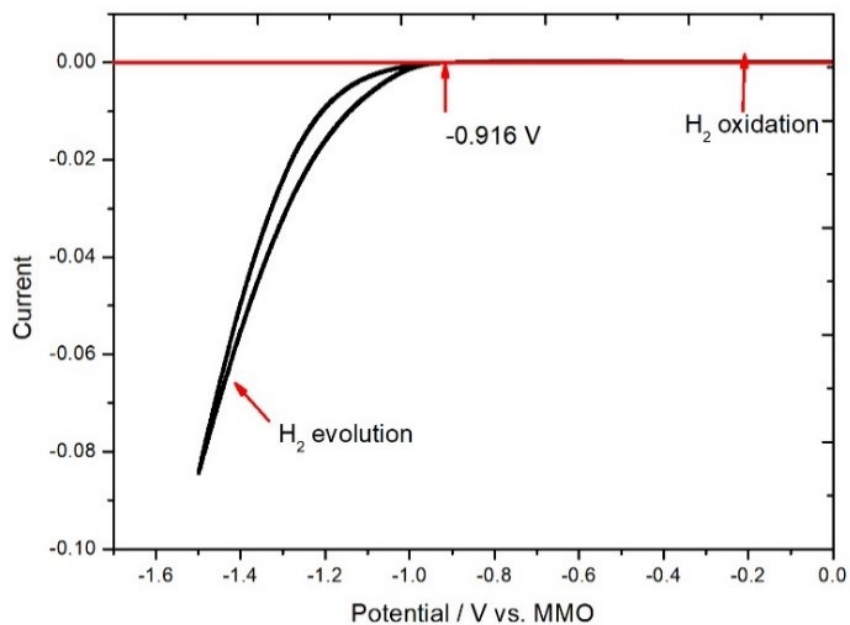
Figure S13. Calibration of mercury/mercury oxide (Hg/HgO) electrode with respect to reversible hydrogen electrode (RHE) in 0.5 M KOH at 10 mV S[-1].

Therefore, we have for 0.5 M KOH:

$$\mathbf{E_{RHE} = E_{Hg/HgO} + 0.916 \ V}$$

The reference electrode (Hg/HgO) used in alkaline medium were calibrated with respect to reversible hydrogen electrode using large area Pt foil as a working and counter electrode. High purity hydrogen gas was purged in the respective solutions for at least 45 min before the experiments and there after a constant overhead purge was maintained during the measurements.[14]

Table S4. The comparison of $(Ba_{0.5}Pb_{1.5})(MgCo)TeB_2O_{10}$ electrocatalyst with reported cobalt substituted metal oxide towards OER.

SI No	Catalyst for OER	Electrolyte Medium	Substrate	Over potential η[V] @ 10 mA*cm^{-2}	Tafel slope [mV dec^{-1}]	Turn over frequency (TOF) S^{-1}	Faradaic efficiency (%)	Reference
1.	IrO_2	1 M KOH	Glassy Carbon	0.338	47	0.01 @300 mV	100	*Nat. Commun.* **2014**, *5*, 4477.
2.	c - Co_3O_4	1 M KOH	Glassy Carbon	0.440	53	0.01 @400 mV	-	*ACS Appl. Energy Mater.* **2020**, *3*(6), 5439−5447.
3.	$NiCo_2O_4$	0.1 M KOH	Glassy Carbon	0.471	161	-	100	Lee, D. U.; et al., *J.Mater.Chem.* **2013**, *1*, 4754-4762.
4.	Nanowire $MnCo_2O_4$	1 M KOH	Carbon Cloth	0.342	115	-	-	*Adv. Funct. Mater.* **2022**, *32* (11), 2107179.
5.	$CoFe_2O_4$	1 M KOH	Carbon Paper	0.477	71	0.000187 @300 mV	-	*ACS Appl. Mater. Interfaces* **2017**, *9*, 13132.
6.	$CoCr_2O_4$	1 M KOH	RDE Glassy Carbon	0.326	51	0.03141 @326 mV	-	*Small.* **2016**, *12*, 2866− 2871.
7.	CoBO NPs			0.359	57	0.0076 @350 mV	-	*Int. J. Hydrogen Energy.* **2018**, *43*, 6138−6149.
	FeBO NPs	1 M KOH	Glassy Carbon	0.390	59	0.0020 @350 mV		
	CoFeBO NPs			0.263	39	0.1029 @350 mV		
8.	$(Ba_{0.5}Pb_{1.5})(MgCo)TeB_2O_{10}$	0.5 M KOH	Glassy Carbon	0.479	73	4.673 @479 mV	96	This work
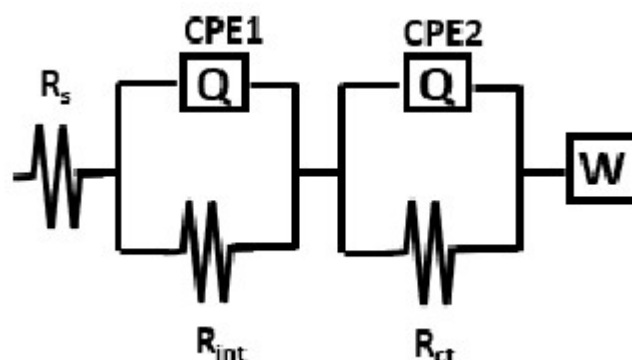
Electrocatalyst	Solution resistance R_s (Ω)	Interfacial contact resistance R_{int} (Ω)	Charge transfer resistance R_{ct} (Ω)	Total resistance (Ω)
C_(Ba$_{0.5}$Pb$_{1.5}$)(MgCo)TeB$_2$O$_{10}$	21.93	25.9	94.08	141.91

This equivalent electrical circuit will try to explain the OER process[15]

- ❖ The R_s (solution resistance) which has contribution from electrode and electrolyte.
- ❖ The CPE1 (constant phase angle element) & R_{int} (interfacial contact resistance) denotes internal double layer polarization and corresponding resistance of the polymeric film on the surface of the electrode.
- ❖ The CPE2 with R_{ct} (charge transfer resistance) was related to faradaic charge transfer resistance was added in the model.
- ❖ Warburg (W) element due to diffusion of electroactive ion at the electrode and electrolyte interface.

Figure S14. The observed equivalent circuit in the electrochemical impedance spectroscopy.
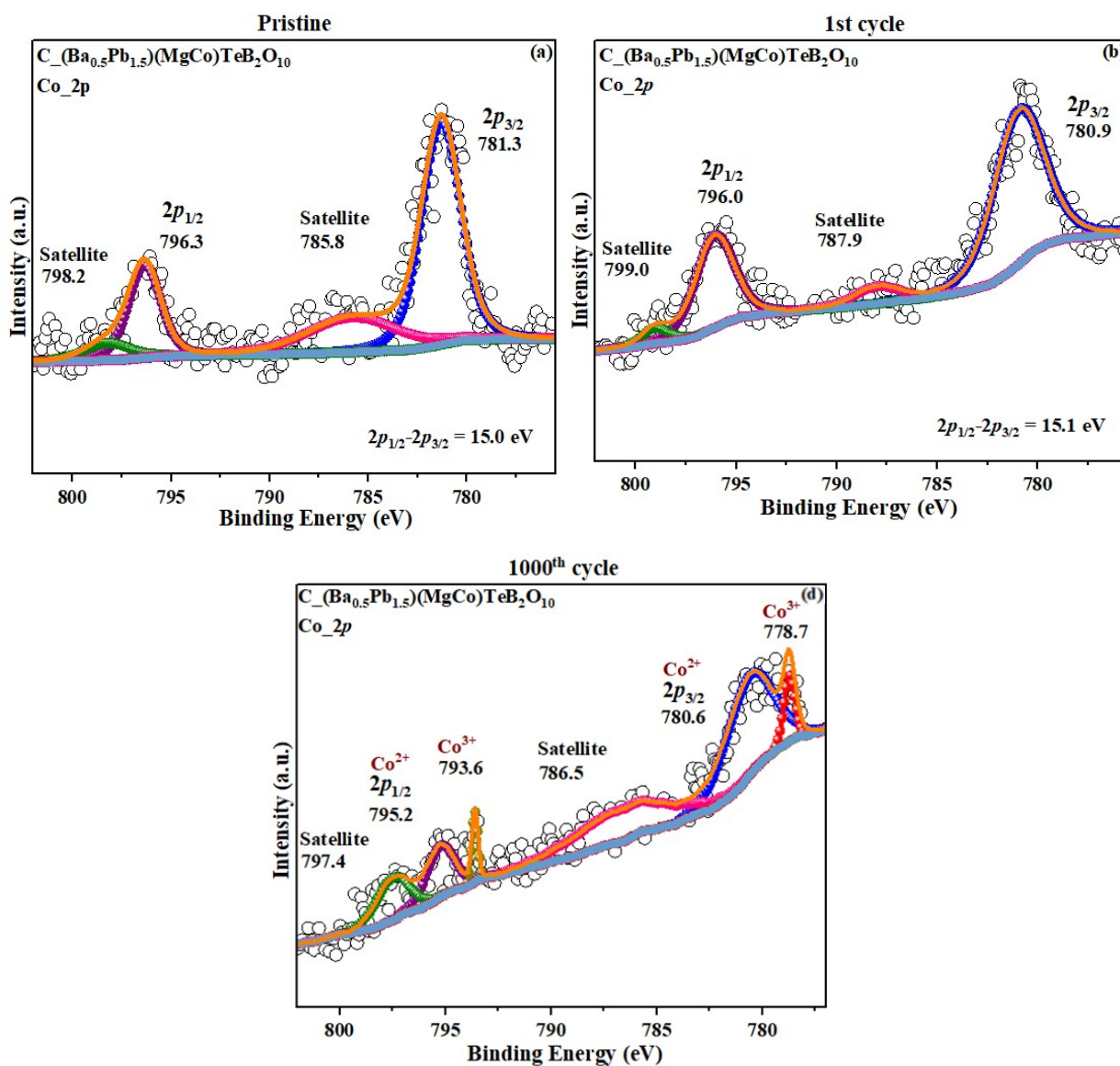
Figure S15. XPS spectra for Co 2p spectra of C_(Ba$_{0.5}$Pb$_{1.5}$)(MgCo)TeB$_2$O$_{10}$ for (a) pristine, (b) 1st cycle (c) 500th cycle, (d) 1000th cycle of cyclic voltammetry scan of the electrocatalyst in 0.5M KOH in the faradaic region.

Table S5. Binding energies of Co $2p$ peaks in the XPS spectra of

Sample Name	Co^{3+} $2p_{3/2}$ (eV)	Co^{3+} $2p_{1/2}$ (eV)	Co^{2+} $2p_{3/2}$ (eV)	Co^{2+} $2p_{1/2}$ (eV)	Satellite
Pristine	---	---	781.3	796.3	785.8/798.2
1st CV	---	---	780.9	796.0	787.9/799.0
1000nd CV	778.7	793.6	780.6	795.2	786.5/797.4

C_(Ba$_{0.5}$Pb$_{1.5}$)(MgCo)TeB$_2$O$_{10}$[16]

Sample Name	Co^{3+}(%)	Co^{2+}(%)	Co^{3+}/Co^{2+}
1000nd CV	06.20	39.14	0.158

$(Ba_{0.5}Pb_{1.5})(MgCo)TeB_2O_{10}$

$(Ba_{0.5}Pb_{1.5})(MgCo)TeB_2O_{10}$

Equation	y = a + b*x
Intercept	0.02788 ± 0.00374
Slope	0.00137 ± 5.538E-5
R-Square (COD)	0.99033

$C\_(Ba_{0.5}Pb_{1.5})(MgCo)TeB_2O_{10}$

$C\_(Ba_{0.5}Pb_{1.5})(MgCo)TeB_2O_{10}$

Equation	y = a + b*x
Intercept	0.01961 ± 0.00876
Slope	0.00475 ± 1.29625E-4
R-Square (COD)	0.99556

S27
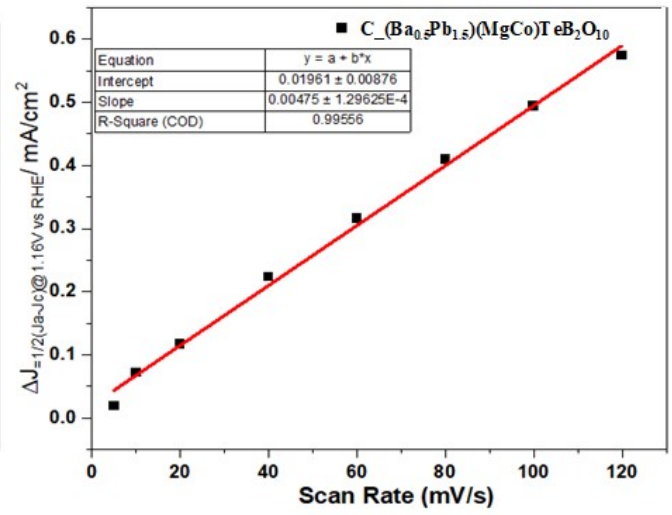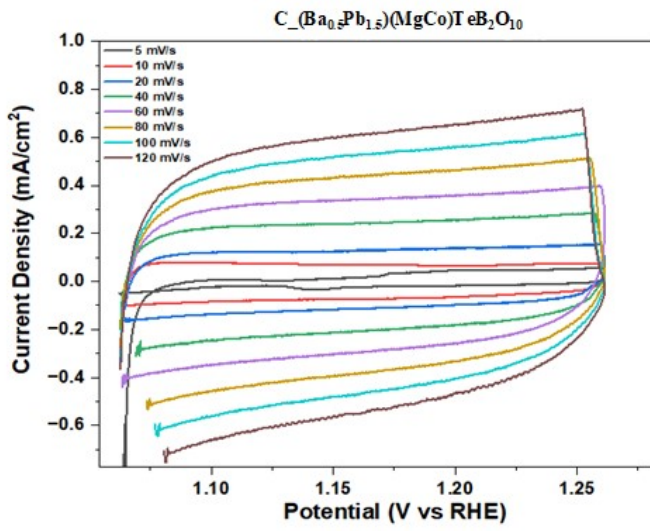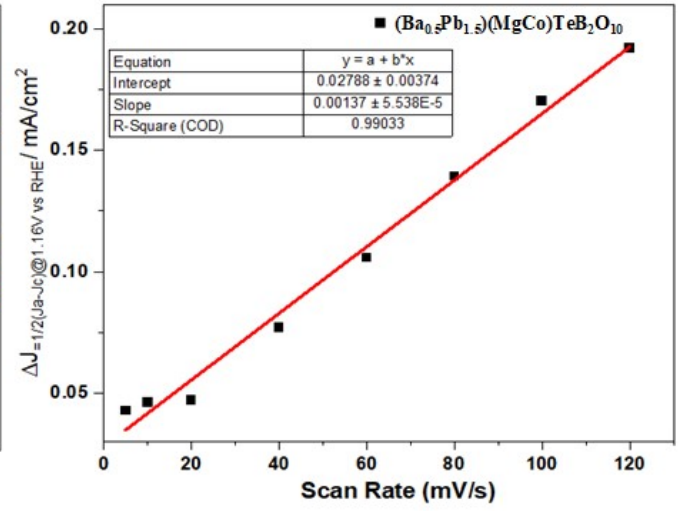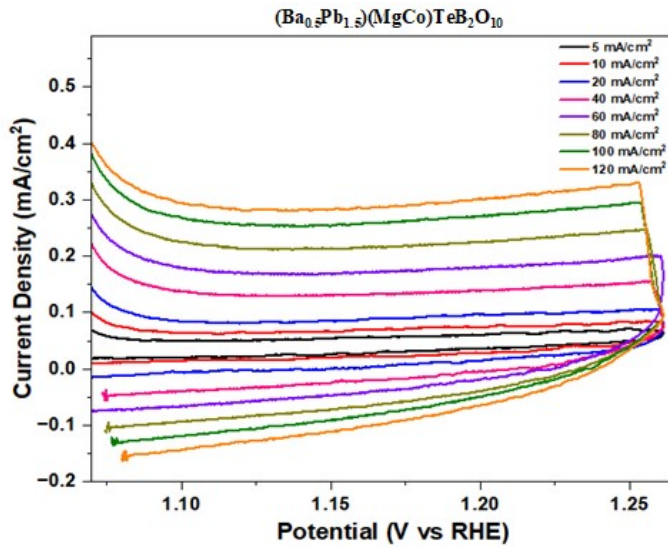
The electrochemically active surface area (ECSA) calculated by the double layer capacitance.[17]

$$ECSA = \frac{Cdl}{Cs}$$

C_{dl} – Double layer capacitance; Cs – Specific capacitance (40 μF/cm^2). Double layer charging current (i_c) is product of scan rate ν (mV/s) and double layer capacitance. If i_c is plotted as a function of ν, then slope will be C_{dl}.

Electrochemically active surface area for $(Ba_{0.5}Pb_{1.5})(MgCo)TeB_2O_{10}$ is 2.418 cm^2 whereas $C\_(Ba_{0.5}Pb_{1.5})(MgCo)TeB_2O_{10}$ is 8.383 cm^2.

Figure S16. Electrochemically active surface area for $C\_(Ba_{0.5}Pb_{1.5})(MgCo)TeB_2O_{10}$

Determination of Turn Over Frequency (TOF) value from OER current[18]

TOF = (i x N$_A$) / (A x F x n x r)

i – current (A); N$_A$ – Avogadro number (6.023 x 10^{23}); A – Geometrical surface area of the working electrode; F – Faraday constant (96485 C / mol); n – Number of electrons involved (n = 4 for OER); r – Surface concentration calculated from LSV redox peak method.

Determination of Surface Concentration of $C\_(Ba_{0.5}Pb_{1.5})(MgCo)TeB_2O_{10}$ from LSV redox peak in the alkaline medium.[19]

Area from Co^{2+} to Co^{3+} redox peak = 5.350 x 10^{-3} V mA; Charge = 5.350 x 10^{-3} V mA / 0.01 V s^{-1} = 5.350 x 10^{-4} Coulombs (q = I x t = A x s); To find number of electron: 5.350 x 10^{-4} C / 1.602 x 10^{-19} C = 3.339 x 10^{15}. The value divide by the 1e$^-$ transfer in the redox reaction gives, 3.339 x 10^{15} atoms.

The OER current of 1 mA/cm^2 observed at 1.560 V *vs*. RHE, 10 mA/cm^2 observed at 1.664 V *vs*. RHE and 40 mA/cm^2 observed at 1.928 V *vs*. RHE.

$$\text{TOF}_{1.56V \, @ \, 1mA/cm^2} = \{(1 \times 10^{-3}) \times (6.023 \times 10^{23})\}/\{(1) \times (96485 \times (4) \times (3.339 \times 10^{15})\} = 0.467 \text{ s}^{-1}.$$

$$\text{TOF}_{1.664V \, @ \, 10mA/cm^2} = 4.673 \text{ s}^{-1}. \quad \text{TOF}_{1.928V \, @ \, 40 \, mA/cm^2} = 18.695 \text{ s}^{-1}.$$
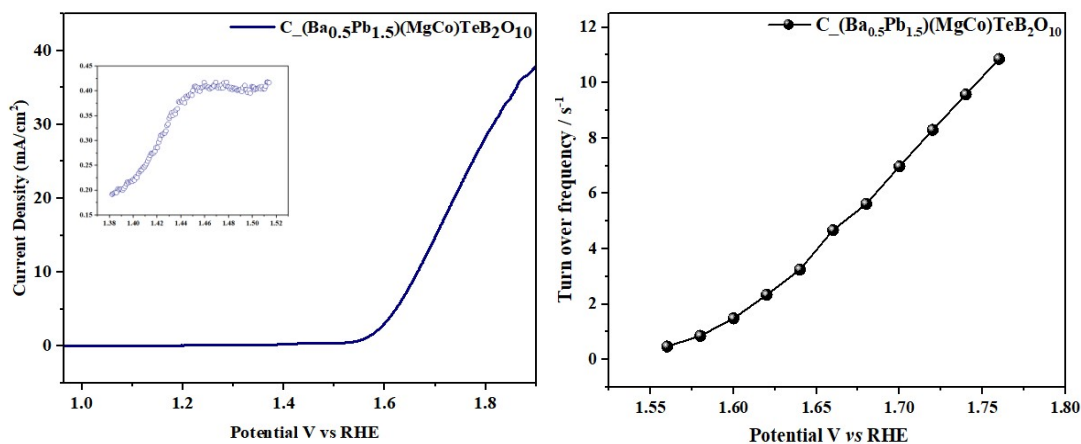
Figure S17. Turn over frequency calculation for $C\_(Ba_{0.5}Pb_{1.5})(MgCo)TeB_2O_{10}$.
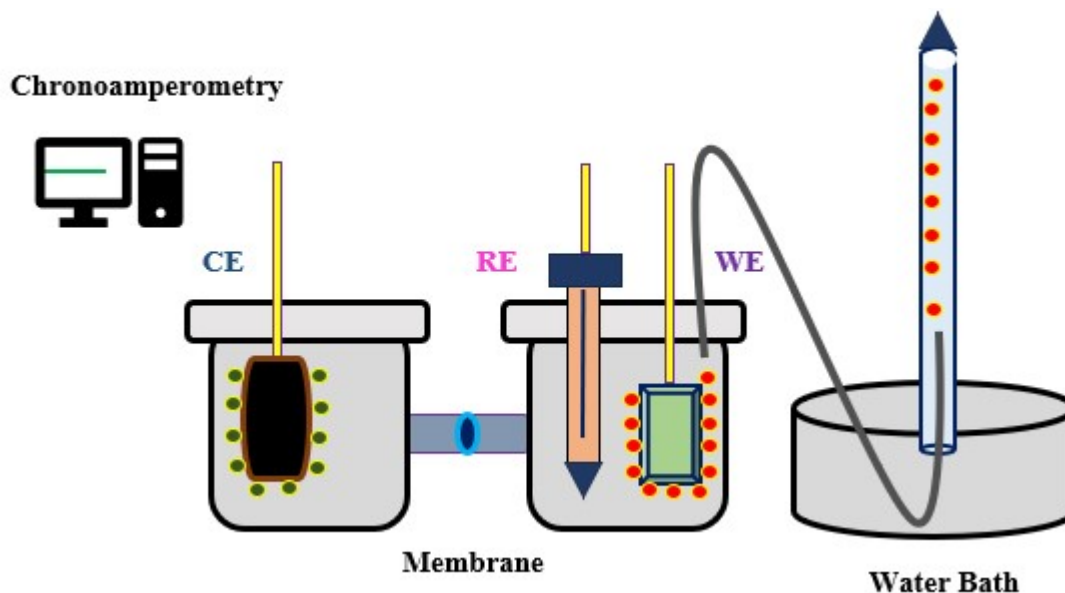
Figure S18. Diagram of inverse burette experimental setup.[20]

We were able to quantified the amount of oxygen gas evolved from alkaline oxygen evolution reaction as a function of time. The chronoamperometric experiment was carried out using H-shaped electrochemical cell as shown in figure S23, to quantify the amount of oxygen gas evolved. The carbon cloth coated with $C\_(Ba_{0.5}Pb_{1.5})(MgCo)TeB_2O_{10}$ and the WE was kept in one compartment of H-shaped cell along with reference electrode (Hg – HgO electrode). A large area counter electrode (graphite rod) was kept in the other compartment. The quantity of oxygen gas evolved was measured using inverse burette method.
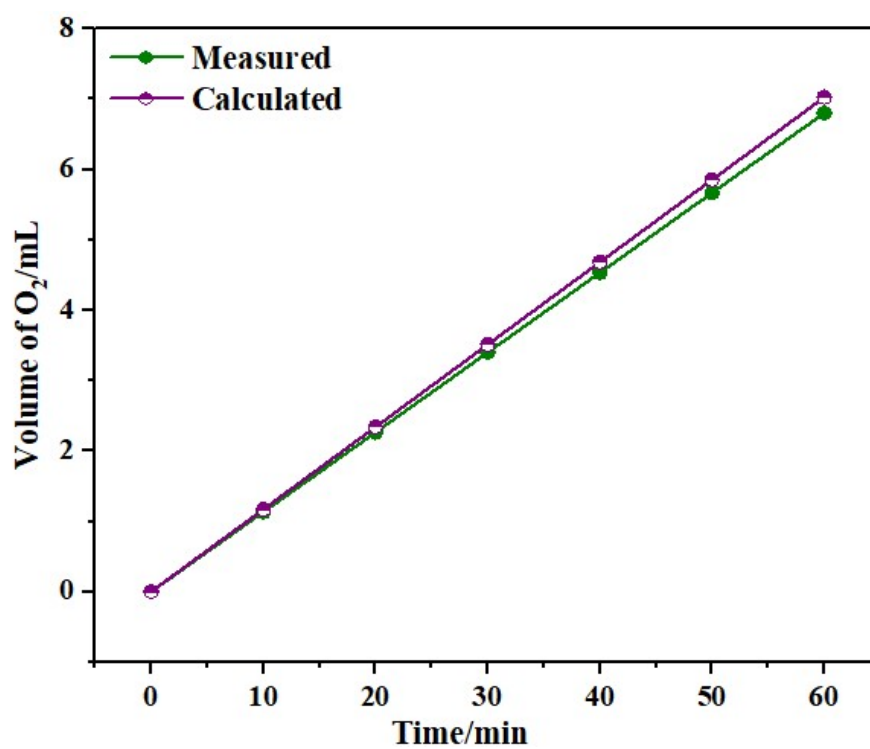
Figure S19. Oxygen production efficiency of C_$(Ba_{0.5}Pb_{1.5})(MgCo)TeB_2O_{10}$.

Measured vs. calculated actual oxygen production catalysed by C_$(Ba_{0.5}Pb_{1.5})(MgCo)TeB_2O_{10}$ after a pretreatment of 30 min. The calculated data represents the expected amount of O_2 gas assuming a quantitative faradaic yield for oxygen gas formation in alkaline medium.
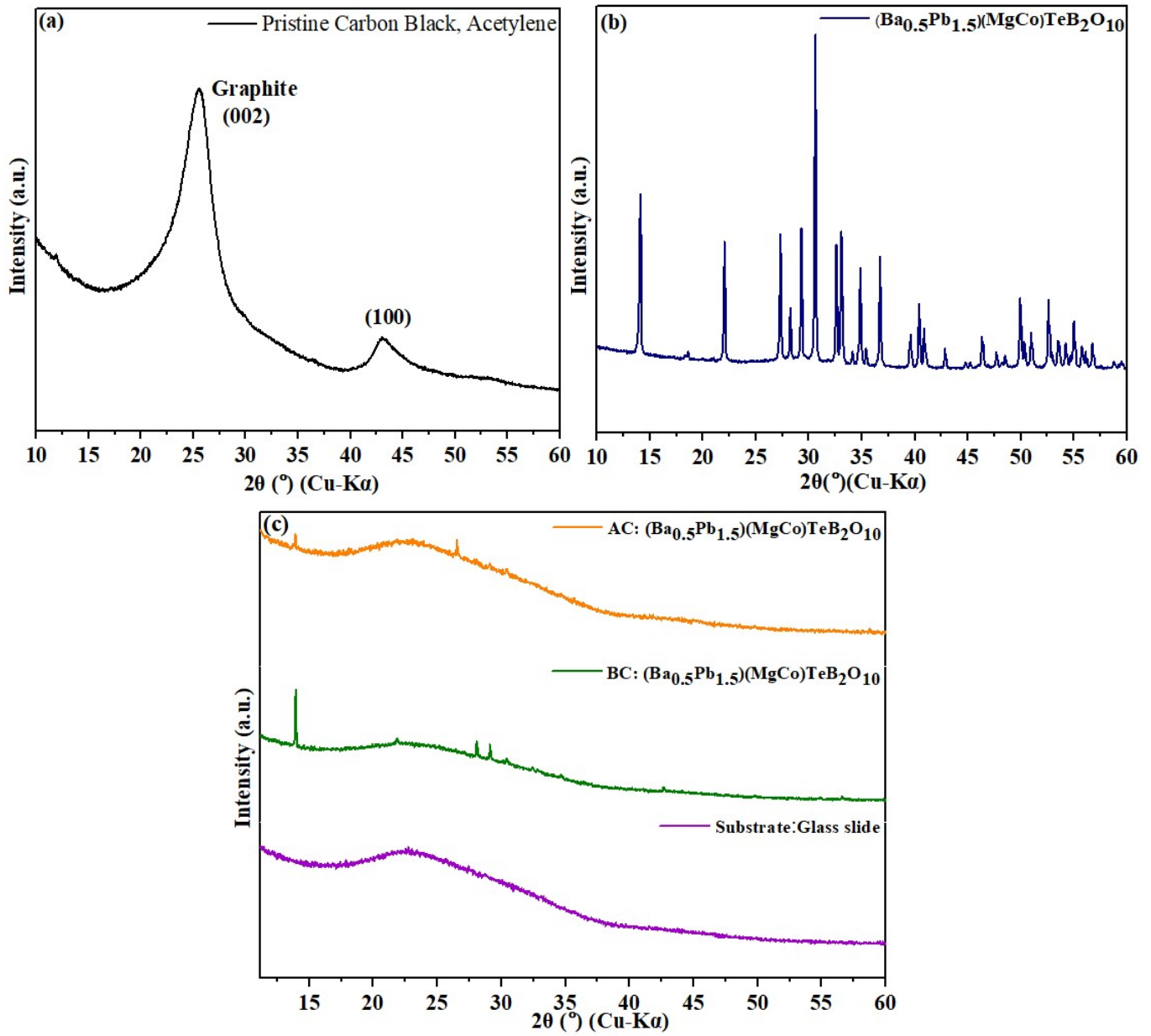
Entry	Ratio of 1a:2	Yield (%) 3a	Yield (%) 4a
1	2:1	45	15
2	1:1	55	10
3	1:2	60	05
4	**1:3**	**75**	**trace**

To check the material stability, before and after electrocatalysis, performed PXRD pattern, after electrocatalysis is 1000 cycle of cyclic voltammetry (scan rate: 10 mV/s) in the faradaic region.

Figure S20. The PXRD (a) Pristine Carbon Black, Acetylene (b) $(Ba_{0.5}Pb_{1.5})(MgCo)TeB_2O_{10}$ (c) Before and after electrocatalysis
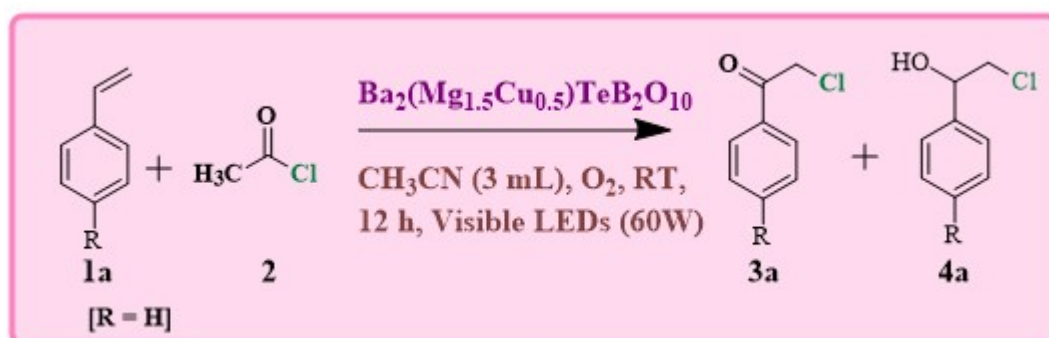
Table S6. Optimised reaction condition: screening of starting materials ratio
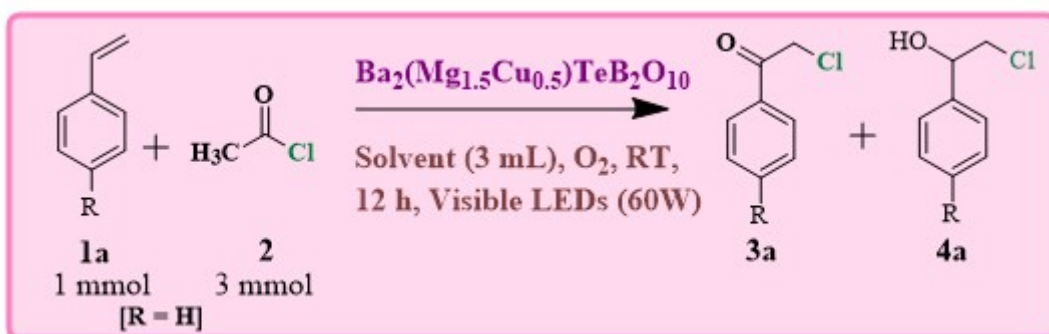
Table S7. Optimised reaction condition: solvent screening

Entry	Solvent	Yield (%) 3a	Yield (%) 4a
1	**Acetonitrile**	**75**	**trace**
2	Ethanol	49	12
3	Methanol	45	11
4	Isopropyl alcohol	48	08
5	Tetrahydrofuran	10	06
6	Dimethyl formamide	05	trace
7	Dichloromethane	08	10
8	1,2-Dichloroethane	10	15
9	Dimethylacetamide	05	trace
10	1,4-Dioxane	14	trace
11	Water	0	0
12	Dimethyl sulfoxide	0	0
13	Ethyl acetate + Isopropyl alcohol (9:1)	20	05

Table S8. Control experiments for oxochlorination of vinyl arene

Entry	Photocatalyst Ba$_2$(Mg$_{1.5}$Cu$_{0.5}$)TeB$_2$O$_{10}$	Visible LED	O$_2$ Gas	Yield (%) 3a
1	✗	✓	✓	trace
2	✓	✗	✓	18
3	✓	✓	✗	30
4	✓	✗	✗	10
5	✗	✓	✗	trace
6	✗	✗	✓	trace
7	✗	✗	✗	trace
8	**✓**	**✓**	**✓**	**75**
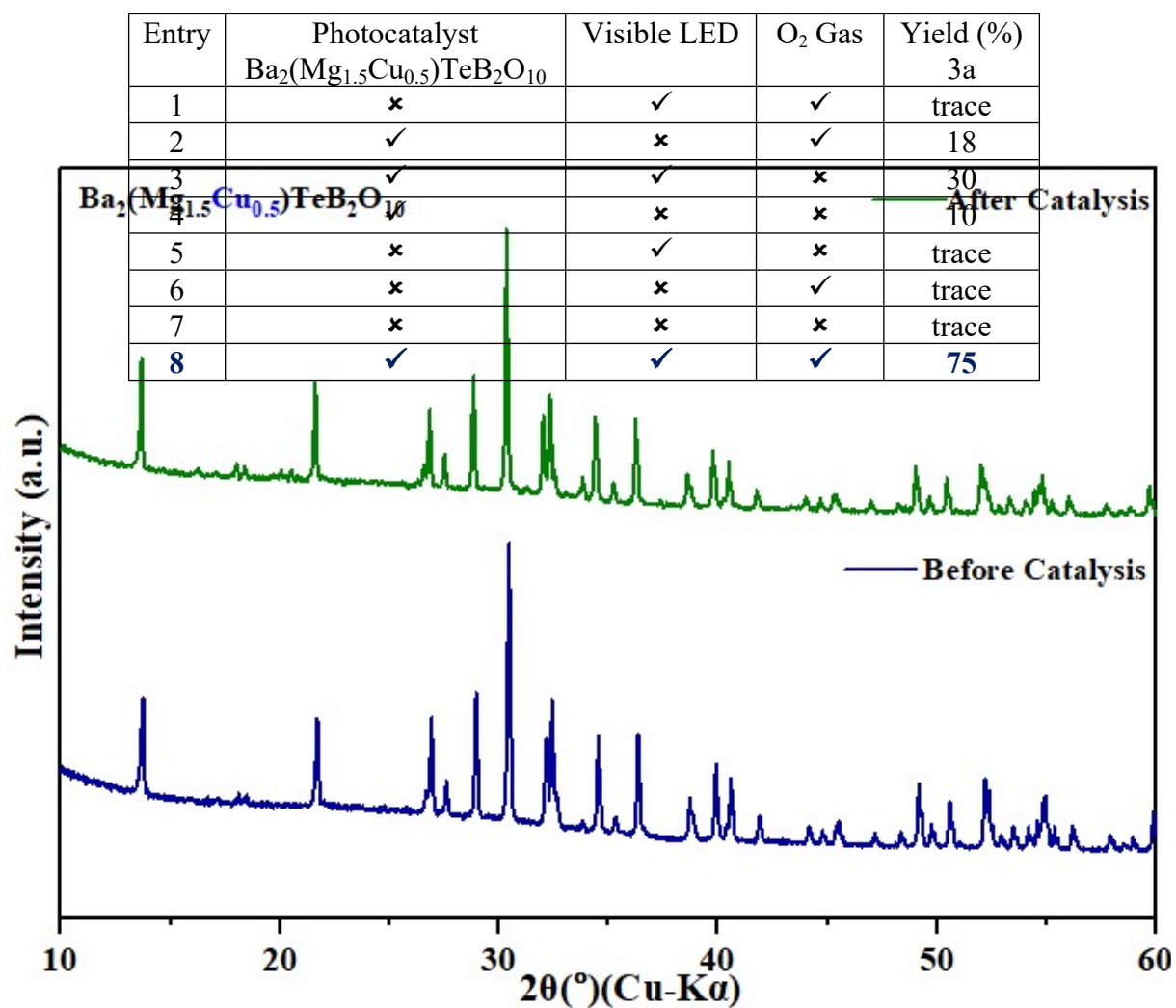
Figure S21. PXRD Pattern of Ba$_2$(Mg$_{1.5}$Cu$_{0.5}$)TeB$_2$O$_{10}$ before and after photocatalysis.
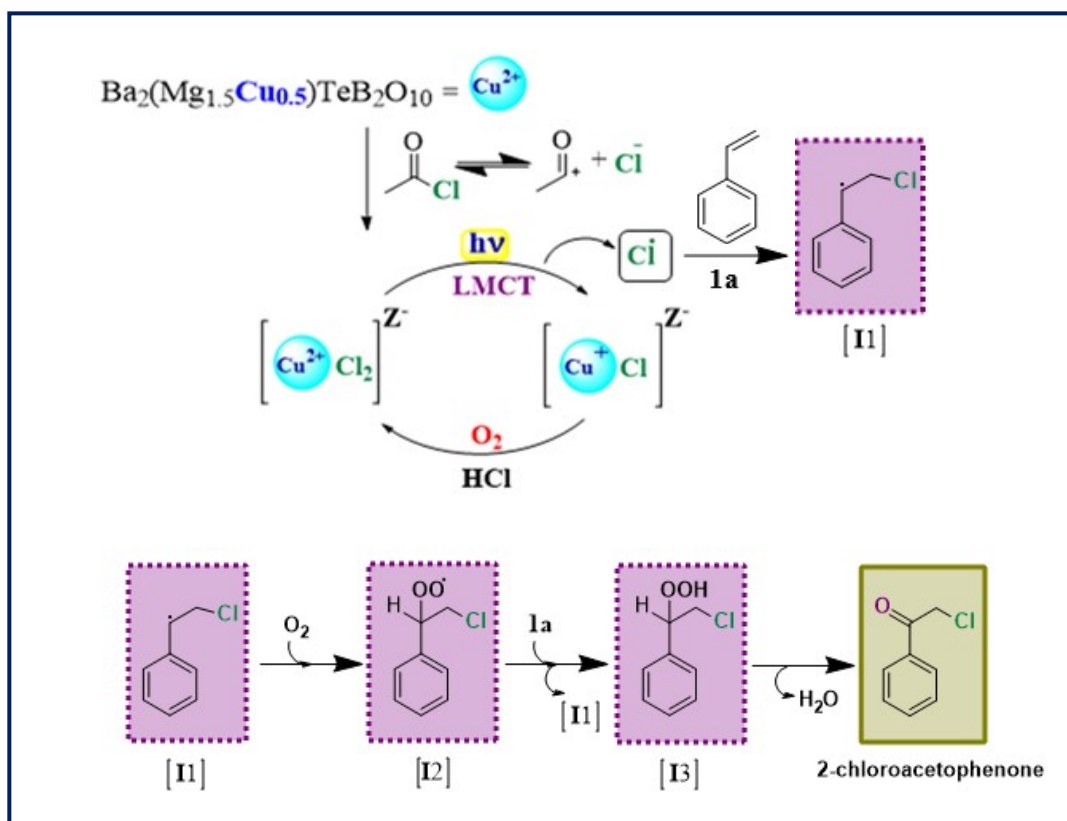
Figure S22. The proposed reaction mechanism for the photocatalytic oxidative halogenation of vinyl arenes.[21]

Photocatalyst	Chlorine Source	Reaction Condition	Isolated Yield	Ref
Cu-C$_3$N$_4$	NiCl$_2$·6H$_2$O	**410 nm** LED, 1 mL of IPA in 9 mL of EtOAC, RT, Air, 12 h	99%	[21]
CuCl$_2$	MgCl$_2$	**455 nm** LED, TFA, MeCN, O$_2$ or air, 36 h	76%	[22]
[Cu^I(dmp)$_2$]Cl	AcCl	**455 nm** LED, MeCN, RT, Air, 36 h	76%	[23]
[Cu^{II}(dmp)$_2$Cl]Cl	AcCl	**455 nm** LED, MeCN, RT, Air, 36 h	74%	[23]
Ba$_2$(Mg$_{1.5}$Cu$_{0.5}$)TeB$_2$O$_{10}$	AcCl	Visible light LED, MeCN, RT, O$_2$, 12 h	75%	This work

Table S9. The comparison of the literature reported catalyst for the visible light mediated oxochlorination of vinyl arenes

¹H NMR (400 MHz, CDCl₃) spectra (3a-3d)

Figure S23. NMR Spectra of 2-Chloro-1-phenylethan-1-one (3a): Yellow Solid. R_f (10% EtOAc/hexane): 0.38. Purification by column chromatography. **¹H NMR (500 MHz, CDCl₃)**: δ (ppm) 8.03 – 7.91 (m, 2H), 7.62 (dd, J = 10.6, 4.2 Hz, 1H), 7.50 (t, J = 7.8 Hz, 2H), 4.72 (s, 2H). The spectral data of this chemical matches previous work[21].
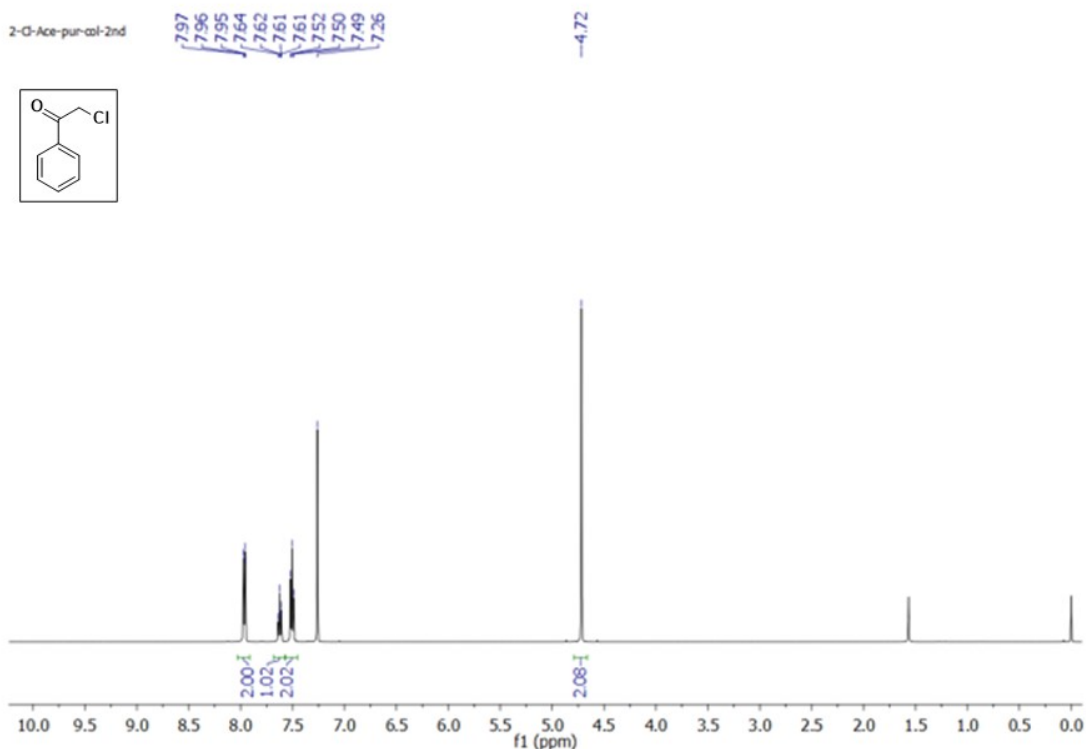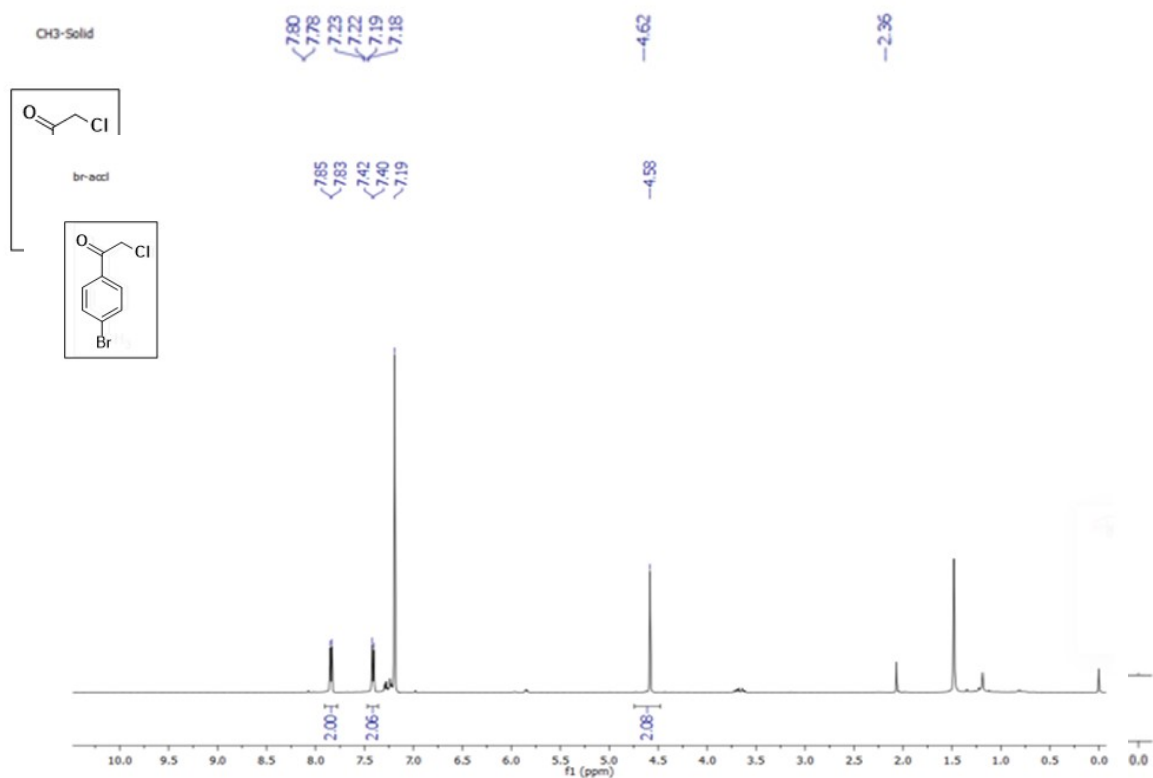

Figure S24. NMR Spectra of 2-Chloro-1-(p-tolyl)ethan-1-one (3b): Colorless Solid. R_f (10% EtOAc/hexane): 0.38. Purification by column chromatography. ¹H NMR (500 MHz, CDCl₃)

δ 7.79 (d, *J* = 8.1 Hz, 2H), 7.22 (d, *J* = 7.9 Hz, 2H), 4.62 (s, 2H), 2.36 (s, 3H). The spectral data of this chemical matches previous work[21].

Figure S25. NMR Spectra of 2-Chloro-1-(4-bromophenyl)ethan-1-one (3c) **:** Colorless Solid. R$_f$ (10% EtOAc/hexane): 0.39. Purification by column chromatography. **¹H NMR (500 MHz, CDCl₃) δ (ppm)** 7.84 (d, J = 8.5 Hz, 2H), 7.41 (d, J = 8.5 Hz, 2H), 4.58 (s, 2H). The spectral data of this chemical matches previous work[21].

Figure S26. NMR Spectra of 2-Chloro-1-(4-chlorophenyl)ethan-1-one (3d): Colorless Solid. R$_f$ (10% EtOAc/hexane): 0.35. Purification by column. **¹H NMR (500 MHz, CDCl₃) δ (ppm)** 7.93 (d, *J* = 8.5 Hz, 1H), 7.50 (d, *J* = 8.5 Hz, 1H), 4.67 (s, 1H). The spectral data of this chemical matches previous work[21].
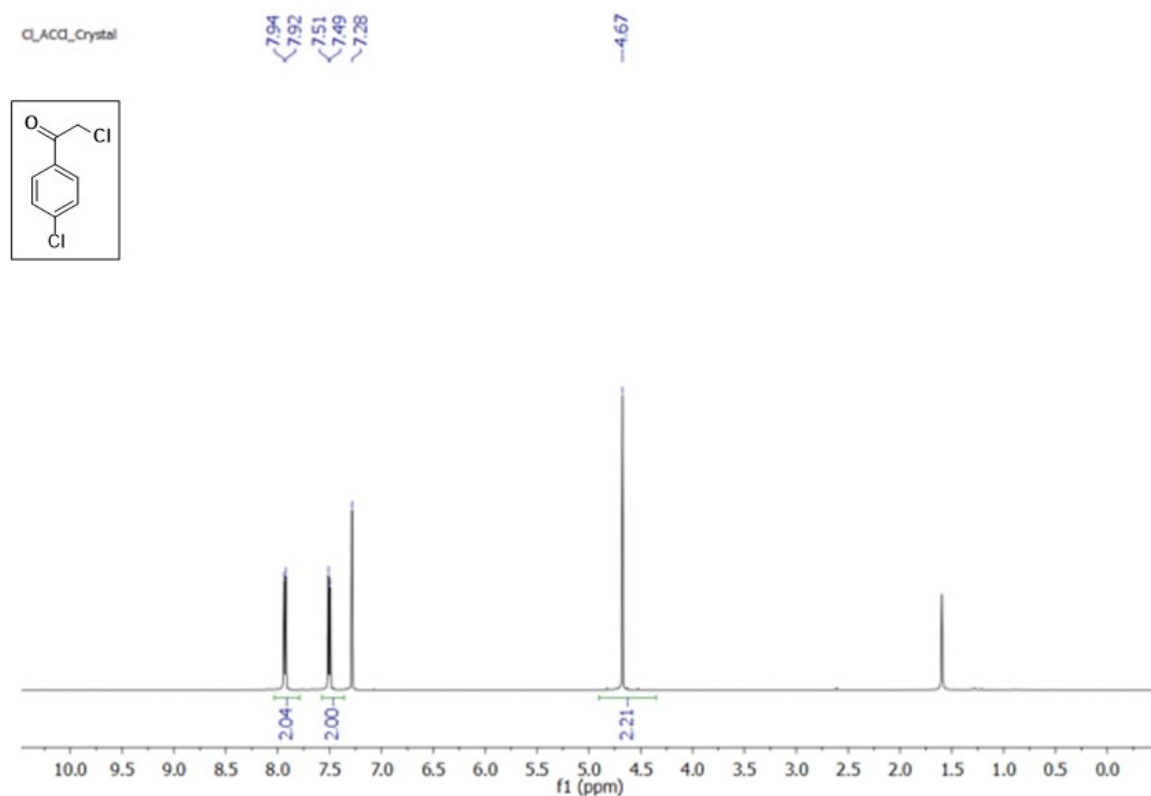
Reference

1   R. A. V. Rossel, R. N. McGlynn and A. B. McBratney, *Geoderma*, 2006, **137**, 70–82.

2   P. Makuła, M. Pacia and W. Macyk, *J Phys Chem Lett*, 2018, 9, 6814–6817.

3   Y. Feng, S. Lin, S. Huang, S. Shrestha and G. Conibeer, *J Appl Phys*.

4   A. J. Bard and L. R. Faulkner, *Surf. Technol*, 1983, **20**, 91–92.

5   D. B. Hibbert and D. B. Hibbert, *Introduction to electrochemistry*, Springer, 1993.

6   D. L. Rousseau, R. P. Bauman and S. P. S. Porto, *Journal of Raman Spectroscopy*, 1981, **10**, 253–290.

7   S. Kesari, R. Rao, M. K. Gupta, R. Mittal and G. Balakrishnan, *Journal of Raman Spectroscopy*, 2019, **50**, 587–594.

8   R. D. Shannon, *J Appl Phys*, 1993, **73**, 348–366.

9   A. B. P. Lever and S. A. Rice, 1969.

10   D. N. Sathyanarayana, *Electronic absorption spectroscopy and related techniques*, Universities Press, 2001.

11   M. Kozielski, I. Pollini and G. Spinolo, *Journal of Physics C: Solid State Physics*, 1972, **5**, 1253.

12   K. B. N. Sarma, B. J. Reddy and S. V. J. Lakshman, *Phys Lett A*, 1982, **92**, 305–308.

13   I. Fontana, A. Lauria and G. Spinolo, *Physica status solidi (b)*, 2007, **244**, 4669–4677.

14   K. Kawashima, R. A. Márquez, Y. J. Son, C. Guo, R. R. Vaidyula, L. A. Smith, C. E. Chukwuneke and C. B. Mullins, *ACS Catal*, 2023, **13**, 1893–1898.

15   D. Tripathy and S. Sampath, *J Power Sources*, 2020, **478**, 229066.

16   J.-C. Dupin, D. Gonbeau, P. Vinatier and A. Levasseur, *Physical Chemistry Chemical Physics*, 2000, **2**, 1319–1324.

17   J.-J. Jow, L.-Y. Hsieh, H.-P. Cho, H.-R. Chen and C.-W. Kuo, *Journal of Industrial and Engineering Chemistry*, 2013, **19**, 1730–1734.

18   S. Anantharaj, P. E. Karthik and S. Kundu, *Catal Sci Technol*, 2017, **7**, 882–893.

19   Y. Yan, X. Ge, Z. Liu, J.-Y. Wang, J.-M. Lee and X. Wang, *Nanoscale*, 2013, **5**, 7768–7771.

20   V. Kiran, D. Mukherjee, R. N. Jenjeti and S. Sampath, *Nanoscale*, 2014, **6**, 12856–12863.

21   F. Han, D. Zhang, S. Salli, J. Ye, Y. Li, F. Rosei, X.-D. Wen, H. Niemantsverdriet, E. Richards and R. Su, *ACS Catal*, 2022, **13**, 248–255.

22   X. He, H. Chang, Y. Zhao, X. Li, S. Liu, Z. Zang, C. Zhou and G. Cai, *Chemistry–An Asian Journal*, 2023, **18**, e202200954.

23   Z. Wang, L. Wang, Z. Wang, P. Li and Y. Zhang, *Chinese Chemical Letters*, 2021, **32**, 429–432.